IEEE Access
Multidisciplinary | Rapid Review | Open Access Journal

Manuscript received November 15, 2016; accepted December 9, 2016, date of publication December 21, 2016, date of current version June 7, 2017.

Digital Object Identifier 10.1109/ACCESS.2016.2642827

Multi-Set Space-Time Shift Keying and Space-Frequency Space-Time Shift Keying for Millimeter-Wave Communications

IBRAHIM A. HEMADEH, (Student Member, IEEE), MOHAMMED EL-HAJJAR, (Senior Member, IEEE), SEUNGHWAN WON, (Senior Member, IEEE), and LAJOS HANZO, (Fellow, IEEE)
School of Electronics and Computer Science, University of Southampton University, Southampton SO17 1BJ, U.K.

Corresponding author: Lajos Hanzo (lh@ecs.soton.ac.uk)

This work was supported in part by EPSRC Project under Grant EP/Noo4558/1 and Grant EP/L018659/1, and in part by the European Research Council's Advanced Fellow Grant under the Beam-Me-Up Project. The research-data of this paper is available at http://dx.doi.org/10.5258/SOTON/403897

ABSTRACT In this paper, we introduce a novel OFDM-aided multifunctional multiple-input multiple-output scheme based on multi-set space-time shift keying (MS-STSK), where the information transmitted over each subcarrier is divided into two parts: STSK codeword and the implicit antenna combination (AC) index. In MS-STSK, a unique combination of antennas can be activated at each subcarrier to convey extra information over the AC index while additionally transmitting the STSK codeword. Furthermore, inspired by the MS-STSK concept, this scheme is extended also to the frequency domain in the novel context of our multi-space-frequency STSK (MSF-STSK), where the total number of subcarriers is partitioned into blocks to implicitly carry the block's frequency index. The proposed MSF-STSK scheme benefits from the huge bandwidths available at mmWaves for partitioning the total number of OFDM subcarriers into blocks to convey more information over the frequency domain. Both proposed systems use STSK codewords as the basic transmission block, and they can achieve higher data throughput and better BER performance than STSK. Moreover, given that the system is meant to operate at mmWaves, antenna arrays relying on several antenna elements are employed at both the transmitter and receiver for analogue beamforming with the aid of phase shifters and power amplifiers to overcome the effect of high path loss.

INDEX TERMS Millimeter waves, wideband channel, MIMO, space-time shift keying, spatial modulation, PSK, QAM.

I. INTRODUCTION

Millimeter wave (mmWave) communications constitutes a promising technique for next-generation wireless communications systems [1], [2]. Due to their huge available bandwidths, mmWaves have been attracting considerable attention with a view to replace or to collectively operate with the saturating sub-3 GHz band [3]. However, as a predicament, mmWaves suffer from high attenuation [4], which fortunately can be mitigated with the aid of accommodating large antenna arrays within relatively small areas for the sake of attaining array gains [5]. As a result for mmWaves, beamforming is considered to be the most suitable multiple-input multiple-output (MIMO) technique.

The family of MIMO schemes devised for wireless communications systems shown in Figure 1 is capable of achieving enhanced transmission rates and an improved communication integrity [6]. For instance, multiplexing techniques, such as the Bell-Labs Layered Space-Time (BLAST) [7] laying under the multiplexing branch of MIMO techniques in Figure 1 are capable of attaining enhanced transmission rates. By contrast, the diversity-oriented MIMO techniques shown in Figure 1, such as Orthogonal Space-Time Block Coding (OSTBC) [8] and its STBC extensions [9] as well as the Space Time Trellis Code (STTC) [10] would achieve diversity gains. Furthermore, Spatial Modulation (SM) [11]–[13] is capable of

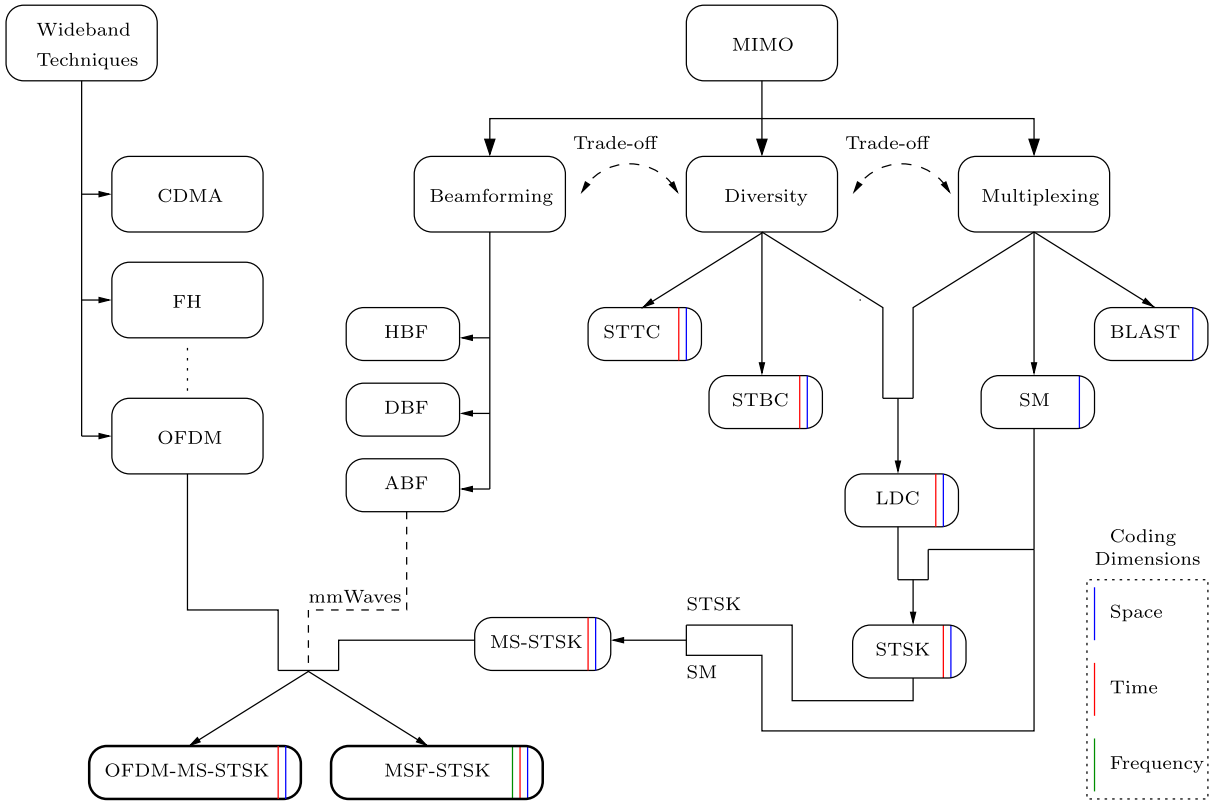

FIGURE 1. Family tree of MS-STSK, OFDM-MS-STSK, and MSF-STSK.

achieving both diversity and multiplexing gains by conveying extra information over the activated transmit antenna index. This scheme was employed successfully for transmission over mmWaves in a Line-of-Sight (LOS) environment [14].

Furthermore, combining two or more MIMO techniques would result in a generalized MIMO scheme referred to as the Multi-Functional (MF) MIMO scheme [15]. MF-MIMOs can be employed for communications over mmWaves, since they are capable of combining the benefits of different MIMO schemes, which is essential for overcoming the high mmWaves attenuation by employing beamforming, whilst simultaneously achieving performance and/or throughput enhancements using diversity and/or multiplexing techniques. An example of MF-MIMOs is constituted by the Layered Steered Space-Time Coding (LSSTC) concept [16], which is capable of achieving a multiplexing gain, diversity gain and Signal-to-Noise (SNR) gain by combining V-BLAST, STBC and Analogue Beamforming (ABF). Another MF-MIMO is the popular Space-Time Shift Keying (STSK) scheme, which was proposed in [17] as a generalized MIMO relative of SM that combines it with Linear Dispersion Codes (LDC) as shown in Figure 1, where instead of activating a single transmit antenna, a single dispersion matrix is activated. This scheme is capable of achieving both multiplexing and diversity gains, whilst striking a compelling trade-off between them. Furthermore, in [18] we proposed an extended STSK referred to as Multi-Set (MS) STSK, where -in addition to the explicit information carried by the STSK codeword- extra information is conveyed implicitly over the index of the activated combination of multiple antennas selected from a higher number of antenna elements.

In [19], we proposed an STSK-based mmWave system for Multi-User (MU) downlink (DL) scenarios. The system considered a wideband mmWave channel, where Orthogonal Frequency Division Multiplexing (OFDM) combined with a digital-analogue hybrid structure is employed for overcoming the effect of the time dispersive multipath channel with the aid of a linear MU-Transmit precoding (MU-TPC) technique used for MU access. Transmitting over wideband channels requires wideband channel techniques, such as Code Division Multiple Access (CDMA), Frequency Hopping (FH) and OFDM [6], as shown in Figure 1. Furthermore, using the aforementioned hybrid architecture is essential for mmWave systems [20], where the digital part provides a high design flexibility in terms of signal processing [21], while the analogue part is capable of compensating for having a reduced number of RF chains by providing high array gains with the aid of large antenna arrays [22]. Hybrid system arrangements are capable of striking an attractive design trade-off between the system performance and the power consumption of high-frequency system components [23].

TABLE 1. Nomenclature.

ABF	Analogue Beamforming	MIMO	Multiple-Input Multiple-Output
AC	Antenna Combination	ML	Maximum Likelihood
AE	Antenna Elements	mmWave	Millimeter Wave
ASU	Antenna Selection Unit	MSF	Multi-Space-Frequency
AWGN	Additive White Gaussian Noise	MS-STSK	Multi-Set Space-Time Shift Keying
BER	Bit Error Rate	MU	Multi-User
BLAST	Bell-Labs Layered Space-Time	OFDM	Orthogonal Frequency-Division Multiplexing
BPC	Bits Per Codeword		
BPC	Bits Per Symbol	OSTBC	Orthogonal STBC
CP	Cyclic Prefix	PSK	Phase-Shift Keying
CSI	Channel State Information	QAM	Quadrature Amplitude Modulation
DAC	Distinct AC	RAA	Receive Antenna Array
FI	Frequency Index	RAE	Receive Antenna Element
GSFIM	Generalized Space-Frequency	SAC	Shared AC
	Index Modulation	SSK	Space-Shift Keying
GSIM	Generalized Spatial Index	ST	Space-Time
	Modulation	STBC	Space-Time Block Code
HL	Hard-Limiter	STSK	Space-Time Shift Keying
ICI	Inter-Channel Interference	SM	Spatial Modulation
LDC	Linear Dispersion Coding	SNR	Signal-to-Noise Ratio
LSSTC	Layered Steered Space-Time	TAA	Transmit Antenna Array
	Coding	TAE	Transmit Antenna Element
MF	Multi-Functional	MU-TPC	MU-Transmit Precoding

In this paper, we propose a pair of system designs for mmWaves, where the digital precoding part of the preferably hybrid beamforming required for increasing the number of data streams transmitted is replaced by applying MIMO signal processing techniques. The first is a novel realization of MS-STSK combined with OFDM for communication over mmWaves referred to as the OFDM-MS-STSK scheme shown in Figure 1. *This space-time subsidized system is capable of striking a trade-off between the achievable throughput and the diversity gains attained, which subsumes the SM [11], STSK [17], and Space-Shift Keying (SSK) [24] schemes as special cases. Using OFDM, the huge mmWave channel bandwidth is partitioned into a high number of narrow sub-bands, where an antenna combination (AC) is activated at each subcarrier to transmit an STSK codeword, hence implicitly transmitting extra information over the activated antenna combination index in addition to the explicit STSK coded bits. The concept of subcarrier indexing was utilized in the OFDM Index Modulation (OFDM-IM) scheme [25] for improving the achievable throughput, where extra information is conveyed over the subcarrier index. This work was later extended both in [26] by introducing an alternative subcarrier grouping technique, and in [27] by advocating a low-complexity optimal detection technique. Furthermore, in [28] the minimum distance of the classic constellation and index-constellation was jointly optimized. Finally, the achievable performance was further improved with the aid of compressed sensing in [29].*

Furthermore, this work is extended to additionally exploit the frequency dimension. The work in [30] applied frequency indexing by transmitting modulated symbols in a unique block pattern. Furthermore, the STSK concept was extended both to Space-Frequency Shift Keying (SFSK) and to Space-Time-Frequency Shift Keying (STFSK) schemes in [31], where the transmitted information is collectively spread over the space, time and frequency domains.

In our second proposed scheme, we present an extended version of the OFDM-MS-STSK technique, where the frequency index is exploited for the sake of implicitly conveying extra information, with the total number of subcarriers being partitioned into blocks of subcarriers and the frequency index of the block is expressed by a unique antenna combination activated at a specific subcarrier. This system is referred to as the Multi-Space-Frequency (MSF) STSK scheme is shown in Figure 1. *Both the proposed systems are combined with analogue beamforming for the sake of mitigating the effect of the high attenuations of mmWaves. As a benefit of the huge available mmWave bandwidth, the channel can be partitioned into a large number of subcarriers, which can benefit the system in terms of many aspects. More specifically, increasing the number of subcarriers would increase the normalized throughput of both proposed systems by reducing the normalized overhead of the long Cyclic Prefix (CP) required at mmWaves* [19], [32]. *Furthermore, as a benefit of reducing the number of subcarriers the number of frequency partitions increases, which thereby implies that the extra information*

conveyed by frequency indexing further increases.

The novel contributions of this paper can be summarized as follows:

- We intrinsically amalgamate the MS-STSK scheme both with OFDM in order to operate over the wideband mmWave channel as well as with beamforming for overcoming the high path loss of the mmWave channel.
- We propose the MSF-STSK concept, where the transmit information is spread over the space-time- and frequency-domains. Hence, additional throughput enhancements may be gleaned from beneficially combining the three domains.

This paper is organized as follows. In Section II, we present the OFDM-MS-STSK system proposed for mmWave communications. Then in Section III, we introduce the extended frequency-domain version of MS-STSK referred to as the MSF-STSK system. Finally, we conclude in Section IV.

Notations: Bold upper case letters represent matrices; $\lfloor . \rfloor$ denotes the flooring of a real number to the nearest smallest following integer, while $\lfloor . \rceil$ denotes the rounding operation of a real number to the nearest integer; $mod(.)$ indicates the modulus operation; $\binom{n}{r}$ denotes the combinations without repetition of n objects taken r at a time; $()^T$ represents the transpose operation and $(.)^H$ represents the Hermitian transpose operation; $\mathbb{C}^{a\times b}$ indicates a matrix of complex numbers of the the size $a \times b$; $\|.\|$ denotes the Frobenius norm and $|.|$ indicates the modulus of a complex number; The $\circledast$ operator denotes the circular convolution operation.

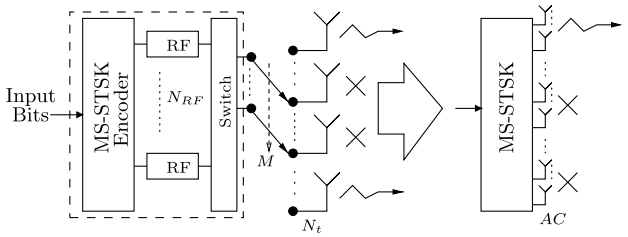

FIGURE 2. MS-STSK transmitter block diagram viewed as an SM-MIMO.

II. MULTI-SET SPACE-TIME SHIFT KEYING SYSTEM FOR MMWAVES

In this section, we intrinsically amalgamate the novel MS-STSK scheme proposed in [18] both with ABF and OFDM for transmission over the mmWave channel. The MS-STSK scheme is an SM-MIMO scheme, where as shown in Figure 2, instead of activating a single transmit antenna in order to implicitly convey the antenna index, a unique, data-specific combination of transmit antennas is activated for transmitting an STSK codeword [17], [33]. STSK is a flexible scheme, where the codewords generated can be flexibly tuned, which could fit any arbitrary transmit antenna size, while striking a trade-off between the achievable diversity gain and the attainable throughput. Different antenna combinations are shown in Figure 2 as a distinct set of multiple antennas. The transmit antennas are spaced far enough to experience independent fading, where the ones activated can be viewed as a distinct set of multiple antennas. The MS-STSK system conveys information over both the STSK codeword and the transmit Antenna Combination (AC) index. An AC is defined as a combination of multiple transmit antennas that are activated to transmit a single STSK codeword.

In order to formulate a symbol set, the number of combinations should ideally be a power of two. This may be achieved either by having a distinct set of AEs for each AC, or with the aid of a distinct combination of AEs out of the total number of available AEs. In the light of this principle, the pair of AC allocation techniques shown in Figure 3 were proposed in [18]. The antenna allocation technique shown in Figure 3(a) is referred to as the Shared Antenna Allocation (SAC) technique, where one or more antenna elements can be shared by several ACs. By contrast, the technique shown in Figure 3(b) is referred to as the Distinct Antenna Allocation (DAC) technique, where M unique AEs are assigned to each AC, i.e. No AEs are shared by the ACs. Furthermore, the general structure of the MS-STSK transmitter is shown in Figure 2, where regardless of the AC allocation technique employed, the MS-STSK transmission mechanism can be characterized by activating one of N_{AC} antenna sets, each formed of M AEs.

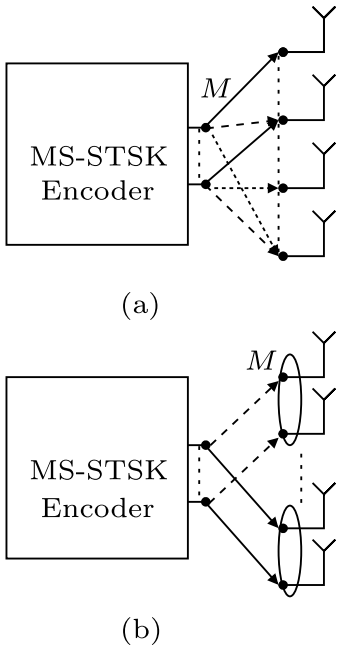

FIGURE 3. MS-STSK block diagram associated (a) with ACs with shared AEs (b) with ACs with distinct sets of AEs.

Owing to the time dispersive and frequency selective nature of mmWave wideband channels [34]–[36], wideband techniques such as OFDM and SC-FDE have to be used for communication over the mmWave channel for the sake of

TABLE 2. List of Symbols.

N_{RF}^{t}	Number of transmitter RF chains	r_{n_r,T_i}	The signal received at the output of the n_r-th receive AE at the T_i MS-STSK time slot
N_t	Number of transmitter antennas		
N_{RF}^{r}	Number of receiver RF chains	h_{n_r,n_t}	Or $h_{n_r,n_t}(t,\tau,\theta,\varphi)$: double-directional CIR
N_r	Number of receiver antennas		
θ_{AC}	Phase shift rotation	N_{sc}	Number of sub-carriers, where $n_{sc}=1,\ldots,N_{sc}$
$\Delta\theta$	Phase-shift difference between two ACs	N_{cp}	CP length
$\mathcal{O}(.)$	Complexity order	$\mathcal{F}_{T_i}$	The T_i-th OFDM symbol
M_Q	Number of dispersion matrices, where $q=1,\ldots,M_Q$	$\mathbf{R}_{T_i}(n_{sc})$	The signal received at the n_{sc}-th sub-carrier within the T_i-th MS-STSK slot
M_c	Constellation size, where $l=1,\ldots,M_c$	$\mathbf{W}(n_{sc})$	ABF precoder at the n_{sc}-th sub-carrier
N_{AC}	Number of combinations, where $n_{AC}=1,\ldots,N_{AC}$	$\mathbf{Z}(n_{sc})$	ABF combiner at the n_{sc}-th sub-carrier
		$\mathbf{R}$	The n_{sc}-th received MS-STSK symbol
N_B	Size of the sub-carriers block, where $n_B=1,\ldots,N_B$	$\hat{\mathbf{H}}(n_{sc})$	The frequency domain of the discrete-time CIR
N_{FI}	The number of ACs dedicated to FI encoding, where $n_{FI}=1,\ldots,N_{FI}$	$\mathbf{H}$	Effective channel observed after applying the transmit and receive ABF
		$\bar{\mathbf{R}}$	Vectorized received signal
T	Number of STSK time slots, where $T_i=1,\ldots,T$	$\bar{\mathbf{H}}$	Vectorized equivalent channel
		$\mathbf{H_c}$	Activated combination effective channel
M	Number of STSK spaces, where $m=1,\ldots,M$	$\mathbf{h}_{c,q}$	The q-th column of the c-th effective channel $\mathbf{H_c}$
B_{ASU}	Number of bits fed into the ASU	$\mathcal{X}$	Vectorized MS-STSK dispersion matrices
B_{STSK}	Number of bits fed into the STSK encoder	$\mathcal{I}$	AC activation matrix
		$\mathbf{I_C}$	Identity matrix at the c-th position in $\mathcal{I}$
$B_{MS-STSK}$	Number of MS-STSK encoded bits	$\mathbf{K}$	QAM/PSK symbol activation vector
		$\triangle\theta_c$	Phase-shift difference between two ACs
B_{FI}	Number of bits used for the FI	$\hat{\mathbf{y}}_{c,q}$	Equalized received signal by the c-th channel combination and the q-th dispersion matrix
$\tilde{\mathbf{X}}$	STSK codeword		
$\mathbf{X}$	MS-STSK codeword		
$\tilde{A}_{q,n_{AC}}$	MS-STSK dispersion matrix	$\hat{s}_l$	The estimate of the l-th transmitted symbol
s_l	QAM/PSK symbol		

mitigating the ISI imposed by the channel. In this study, we employ the OFDM scheme, which subdivides the wideband channel into a large number of orthogonal narrow-band sub-carriers. Together with MS-STSK, extra information carried over the activated AC index may be transmitted over each OFDM subcarrier with the aid of an MS-STSK encoder, which can be used for mapping each STSK codeword at each subcarrier to its corresponding transmit antenna combination. The amalgamated system combination of OFDM and MS-STSK is referred to as OFDM-MS-STSK and in what follows it is invoked for NLOS mmWave scenarios.

The OFDM-aided MS-STSK transmitter referred to as OFDM-MS-STSK is equipped with N_{RF}^{t} Transmit Antenna Arrays (TAAs) for the sake of achieving analogue beamforming, which is a key enabling technology for mmWave systems relying on a pair of phase-shifters and power amplifiers dedicated to each of the Transmit Antenna Elements (TAEs).[1]

[1]Transmit antenna arrays contain multiple AEs used to apply ABF.

Similarly, the receiver is equipped with N_{RF}^{r} Receive Antenna Arrays (RAAs) for the sake of achieving further beamforming gain.

A. OFDM-MS-STSK TRANSMITTER

Consider the OFDM-MS-STSK transmitter shown in Figure 4 equipped with N_{RF}^{t} TAAs and a total of N_t TAEs, where each TAA consists of N_{AA}^{t} antenna array elements for the sake of applying ABF with the aid of a pair of phase-shifters and power amplifiers. The N_{RF}^{t} RF chains comprise all the components needed for baseband to RF up-conversion, including the digital-to-analogue converter, up-conversion, filters, power amplifiers (PA) and low noise amplifiers (LNA) [37]. Hence, reducing the required number of RF chains is desirable for reducing the transmitter's cost. The MS-STSK encoder is fed with a block of $B_{MS-STSK}$ bits, which divides the input bits into B_{STSK} and B_{ASU} bits with the aid of the serial-to-parallel (S/P) converter shown in Figure 4 in order to feed the STSK encoder and multi-set (MS) precoder with their corresponding bit streams.

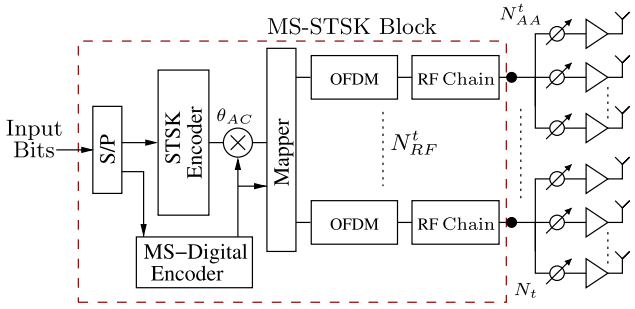

FIGURE 4. Transmitter block diagram of the OFDM-MS-STSK system.

The STSK encoder generates the STSK codeword $\tilde{\mathbf{X}}$ by spreading the $B_{STSK} = \log_2(M_c M_Q)$ number of input bits over T time intervals and M spatial dimensions, where M_c is the QAM/PSK constellation size and M_Q is the total number of dispersion matrices. The STSK codeword is expressed as

$$\tilde{\mathbf{X}} = A_q s_l, \tag{1}$$

where s_l is the M_c-PSK/QAM symbol and $A_q \in \mathbb{C}^{M\times T}$ is the activated dispersion matrix of the dispersion matrix set $\{A_q\}_{q=1}^{M_Q}$. The dispersion matrices are generated based on the random search process described in [33] satisfying the power constraint of $tr\left(A_q^H A_q\right) = T$ for $q = 1, \ldots, M_Q$.

As shown in Figure 4, the S/P converter located at the transmitter's input provides the MS-Digital precoder with B_{AS} bits used for mapping the STSK codeword to its corresponding transmit AC. Based on a bit-to-AC look-up table [18], the MS encoder applies a phase-shift of θ_{AC} to the modulated symbol s_l and maps the STSK codeword to its appropriate AC, regardless of the AC allocation technique employed, where a zero phase-shift is applied for MS-STSK encoding associated with the DAC.

The total number of ACs in the classical MS-STSK scheme presented in [18] relies on both the total number of AEs and the size of M. By contrast, the total number of ACs in the OFDM-MS-STSK scheme is jointly determined by the total number of TAAs and the size of M, since each TAA of size N_{RF}^{t} AEs carries a single stream, while in the classical MS-STSK scheme the streams are transmitted by each TAE. Hence, the total number of encoded bits characterizing the AC indices can be expressed as

$$B_{ASU} = \left\lfloor \log_2 \binom{N_{RF}^{t}}{M} \right\rfloor, \tag{2}$$

for OFDM-MS-STSK associated with SAC and as

$$B_{ASU} = \log_2 \left(\frac{N_{RF}^{t}}{M} \right), \tag{3}$$

for OFDM-MS-STSK associated with DAC.

The SAC technique represents the general AC allocation technique of MS-STSK, which includes the DAC technique as a special case [18]. Hence, we consider it as the main AC allocation technique for the sake of reducing the total number of RF chains required for achieving a specific throughput. The DAC technique would require a higher number of TAAs than the SAC to achieve a specific throughput, which would impose an increased terminal cost as a result of the increased number of RF chains.

When the same TAA participates in multiple ACs, an interdependence is introduced between them [18], [38], hence a phase shift $\theta_{n_{AC}}$ is applied to each STSK codeword in order to overcome the correlation introduced by the common TAAs in different ACs. In MS-STSK [18], each AC is given a predefined phase-shift based on the modulation scheme adopted. The phase shift mainly rotates the symbol constellation used, hence the rotated MS-STSK codeword can be expressed as

$$\begin{aligned} \mathbf{X} &= \left(\tilde{A}_q s_l\right) e^{j\theta_{n_{AC}}} && (4)\\ &= \tilde{A}_{q,n_{AC}} s_l && (5)\\ &= [\mathbf{x_1} \ldots \mathbf{x_{n_t}} \ldots \mathbf{x_{N_t}}]^T \\ &= [\mathbf{X_1} \ldots \mathbf{X_{T_i}} \ldots \mathbf{X_T}], \end{aligned}$$

where $\tilde{A}_q \in \mathbb{C}^{N_{RF}^{t}\times T}$ denotes the MS-STSK dispersion matrix representing the equivalent mapped version of A_q, $\tilde{A}_{q,n_{AC}} \in \mathbb{C}^{N_{RF}^{t}\times T}$ represents the MS-STSK dispersion matrix representing the q-th STSK dispersion matrix and the n_{AC}-th AC, $\mathbf{x_m} \in \mathbb{C}^{1\times T}$ represents the n_{RF}^{t}-th row of the codeword $\mathbf{X}$ given that $n_{RF}^{t} = 1, \ldots, N_{RF}^{t}$, where finally, $\mathbf{X_{T_i}} = [X_{T_i,1} \ldots X_{T_i,m} \ldots X_{T_i,M}]^T \in \mathbb{C}^{M\times 1}$ is the T_i-th column representing the T_i-th time slot of the codeword $\mathbf{X}$.

Again in order to overcome the frequency selectivity of the wideband mmWave channel, OFDM is employed based on the OFDM-aided STSK mapping technique in [32]. Prior to the MS encoding, a total of N_{sc} STSK codewords are fed into the space-time mapper of Figure 4 in order to generate T OFDM symbols carrying the N_{sc} codewords. As shown in Figure 5, the T_i-th OFDM symbol can be expressed as

$$\mathcal{F}_{T_i} = \left[\mathbf{X}_{T_i}(1) \ldots \mathbf{X}_{T_i}(n_{sc}) \ldots \mathbf{X}_{T_i}(N_{sc})\right] \in \mathbb{C}^{N_{RF}^{t}\times N_{sc}}, \tag{6}$$

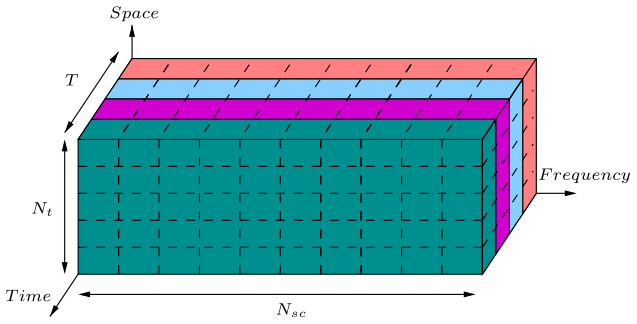

FIGURE 5. Transmitted OFDM symbols over the T STSK time slots.

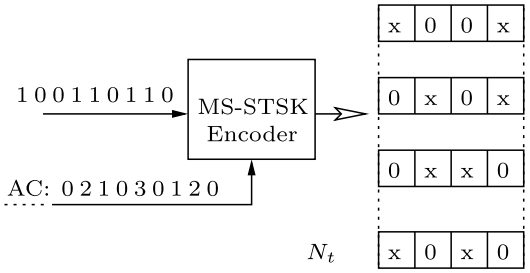

FIGURE 6. MS-STSK codeword at each subcarrier is mapped to its corresponding TAAs based on the AC N_{sc} sequence fed from the MS encoder.

where $T_i = 1, \ldots, T$ represents the STSK time slot, $n_{sc} = 1, \ldots, N_{sc}$ denotes the n_{sc}-th subcarrier, N_{sc} denotes the total number of subcarriers and finally, $\mathbf{X}_{T_i}(n_{sc})$ represents the T_i-th component of n_{sc}-th MS-STSK codeword $\mathbf{X}(n_{sc})$ defined in (1). Furthermore, the n^t_{RF}-th component of $\mathbf{X}_{T_i}(n_{sc})$ is denoted by $\mathbf{X}_{T_i,n^t_{RF}}(n_{sc})$, hence $\mathbf{X}_{T_i}(n_{sc}) = [\mathbf{X}_{T_i,1}(n_{sc}) \ldots \mathbf{X}_{T_i,n^t_{RF}}(n_{sc}) \ldots \mathbf{X}_{T_i,N^t_{RF}}(n_{sc})]^T$.

TABLE 3. AC mapping table of a transmitter equipped with $N^t_{RF} = 4$ and STSK encoder associated with $M = 2$, where TAA_i corresponds to the TAA's index.

AC	TAA Combination
0	$\{TAA_1, TAA_2\}$
1	$\{TAA_1, TAA_3\}$
2	$\{TAA_1, TAA_4\}$
3	$\{TAA_2, TAA_3\}$

The MS encoder collects N_{sc} AC indices in order to map each AC to its corresponding n_{sc} subcarrier, based on the predefined look-up table. For example, the AC mapping scheme shown in Table 3 is that of a transmitter equipped with a total of $N^t_{RF} = 4$ TAAs and an STSK encoder associated with $M = 2$, where the total number of ACs is equal to $N_{AC} = 4$ ACs. In this example, if the ASU produced the AC index of 2, then TAA_1 and TAA_4 are activated in order to transmit the data at the n_{sc}-th subcarrier, while when the ASU produces the AC index of 3, TAA_2 and TAA_3 are activated instead, as shown in Table 3.

An example schematic of the mapping procedure of different ACs to several subcarriers is shown in Figure 6, where the input bits are encoded using the MS-STSK encoder. Afterward, each STSK codeword is mapped to its corresponding TAAs.

The output of the n^t_{RF}-th OFDM modulator is defined as:

$$\bar{x}_{T_i,n^t_{RF}}[n_{sc}] = \sqrt{N_{sc}}.IDFT\left\{\mathbf{X}_{T_i,n^t_{RF}}(n_{sc})\right\}. \quad (7)$$

Due to the short wave-lengths of mmWave signals, large numbers of AEs may be accommodated in relatively compact spaces for the sake of achieving high ABF gains, which is imperative for mitigating the high path loss of mmWaves [35]. The OFDM-MS-STSK system proposed here may be readily operated in the 28 GHz, 38 GHz, 60 GHz or 72 GHz frequency bands having wavelengths of 10.7 mm, 7.9 mm, 5 mm and 4.2 mm, respectively. Each AE in the TAA is connected to a phase-shifter and an amplifier, which steers the signal towards the receiver. For instance, at the n^t_{RF} TAA, a steering vector of $\mathbf{w}(\theta^{Tx}_{n^t_{RF}}) = [w(\theta^{Tx}_{n^t_{RF},1}) \ldots w(\theta^{Tx}_{n^t_{RF},N^t_{AA}})]^T \in \mathbb{C}^{N^t_{AA}\times 1}$ steers the output of the TAA, where the overall ABF precoder at the n_{sc}-th subcarrier can be expressed as

$$\mathbf{W}(n_{sc}) = \begin{bmatrix} \mathbf{w}(\theta^{Tx}_1) & \mathbf{0} & \mathbf{0} & \cdots & \mathbf{0} \\ \mathbf{0} & \ddots & \vdots & \vdots & \mathbf{0} \\ \mathbf{0} & \mathbf{0} & \mathbf{w}(\theta^{Tx}_{n^t_{RF}}) & \cdots & \vdots \\ \vdots & \vdots & \vdots & \ddots & \vdots \\ \mathbf{0} & \mathbf{0} & \mathbf{0} & \mathbf{0} & \mathbf{w}(\theta^{Tx}_{N^t_{RF}}) \end{bmatrix}, \quad (8)$$

where $\mathbf{W}(n_{sc}) \in \mathbb{C}^{N_t\times N^t_{RF}}$ and $\mathbf{0}$ is a vector of zeros. The AEs of each TAA are spaced at a distance of $\lambda/2$ in order to achieve a BF gain. Furthermore, the steering vectors of inactivate antennas are zeros.

B. MS-STSK RECEIVER

The OFDM-MS-STSK receiver's block diagram is shown in Figure 7. The receiver is equipped with N^r_{RF} RAAs with an identical number of RF chains. Each RAA is formed of N^r_{AA} AEs employed for the sake of achieving a further receive ABF gain. The n^r_{RF}-th RAA ABF weights vector $\mathbf{z}(\theta^{Rx}_{n^r_{RF}}) = [z(\theta^{Rx}_{n^r_{RF},1}) \ldots z(\theta^{Rx}_{n^r_{RF},N^r_{AA}})] \in \mathbb{C}^{1\times N^r_{AA}}$ can be generalized for all the N^r_{RF} RAAs at subcarrier n_{sc} as

$$\mathbf{Z}(n_{sc}) = \begin{bmatrix} \mathbf{z}(\theta^{Rx}_1) & \mathbf{0} & \mathbf{0} & \cdots & \mathbf{0} \\ \mathbf{0} & \ddots & \vdots & \vdots & \mathbf{0} \\ \mathbf{0} & \mathbf{0} & \mathbf{z}(\theta^{Rx}_{n^r_{RF}}) & \cdots & \vdots \\ \vdots & \vdots & \vdots & \ddots & \vdots \\ \mathbf{0} & \mathbf{0} & \mathbf{0} & \mathbf{0} & \mathbf{z}(\theta^{Rx}_{N^r_{RF}}) \end{bmatrix}, \quad (9)$$

where $\mathbf{Z}(n_{sc}) \in \mathbb{C}^{N^r_{RF}\times N_r}$ represents the ABF weights vector at the n_{sc}-th subcarrier and $\mathbf{0}$ is a vector of zeros.

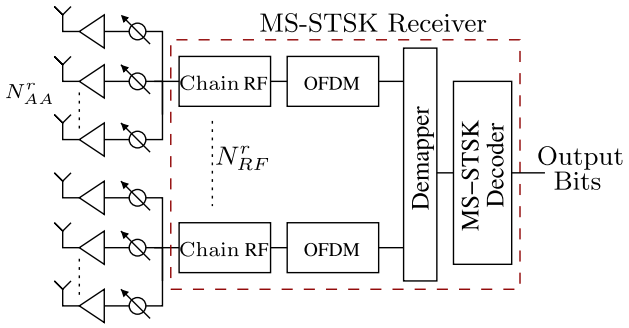

FIGURE 7. OFDM-MS-STSK receiver block diagram.

It was shown in [39]–[42] that the mmWave channel can be represented by a clustered multipath channel model, where different multipath components propagate in distinct clusters segregated both in space and time, as governed by the angle-of-departure (AoD), angle-of-arrival (AoA) and the delay characteristics. The mmWave channel between the n_t-th TAE and the n_r-th receive AE is characterized by the double-directional impulse response [34], [39] as

$$\begin{aligned} h_{n_r,n_t}(t,\tau,\theta,\varphi) = \sum_{n_c=1}^{N_{cl}} \sum_{n_p=1}^{N_p(n_c)} \alpha_{n_c,n_p} \\ .\delta(\varphi - \bar{\varphi}^{Rx}_{n_c} - \varphi^{Rx}_{n_c,n_p}) \\ .\delta(\theta - \bar{\theta}^{Rx}_{n_c} - \theta^{Rx}_{n_c,n_p}) \\ .\delta(\varphi - \bar{\varphi}^{Tx}_{n_c} - \varphi^{Tx}_{n_c,n_p}) \\ .\delta(\theta - \bar{\theta}^{Tx}_{n_c} - \theta^{Tx}_{n_c,n_p}) \\ .\delta(t - \tau_{n_c} - \tau_{n_c,n_p}), \end{aligned} \tag{10}$$

where α_{n_c,n_p} is the complex gain of the n_p-*th* multipath component in the n_c-*th* cluster. Both $(\theta^{Tx}_{n_c,n_p}, \theta^{Rx}_{n_c,n_p})$ and $(\varphi^{Rx}_{n_c,n_p}, \theta^{Rx}_{n_c,n_p})$ characterize the (azimuth, elevation) AoD and AoA at the transmitter and receiver, respectively, given that $(\bar{\varphi}^{Tx}_{n_c}, \bar{\theta}^{Tx}_{n_c})$ and $(\bar{\varphi}^{Rx}_{n_c}, \bar{\theta}^{Rx}_{n_c})$ represent their corresponding mean cluster angles. The parameter τ_{n_c,n_p} denotes the delay of the n_p-*th* multipath component in the n_c-*th* cluster and τ_{n_c} is the n_c-*th* cluster delay. Hence, the discrete-time CIR of the mmWave channel between the transmitter and receiver may be expressed as

$$\hat{H}[n_{sc}] = \sum_{n_p=0}^{\bar{N}_p-1} \hat{H}[n_p]\delta[n_{sc} - n_p], \tag{11}$$

where $\hat{H}[n_{sc}]$ is a simplified representation of (10), which denotes all sub-paths of all clusters in $\bar{N}_p$, given that $\bar{N}_p = \sum_{n_c=1}^{N_{cl}} \sum_{n_p=1}^{N_p(n_c)} 1$. Furthermore, a single coefficient of the matrix $\hat{H}[n_p]$ represents the channel between the n_t-th TAE and the n_r-th receive AE, and it is denoted by $\hat{h}_{n_r,n_t}[n_p]$. Hence, the signal received at the output of the n_r-th receive AE at the T_i STSK time slot can be expressed as

$$\begin{aligned} r_{n_r,T_i}[n_{sc}] = \sum_{n_t=1}^{N_t} \sum_{n_p=0}^{\bar{N}_p-1} \hat{h}_{n_r,n_t}[n_p] \circledast \bar{x}_{T_i,n_t}[n_{sc} - n_p] \\ + v_{T_i}[n_{sc}], \end{aligned} \tag{12}$$

where $\bar{x}_{T_i,n_t}[n_{sc}]$ is the STSK symbol transmitted by the n_t-th AE at the T_i STSK time slot, $v_{T_i}[n_{sc}]$ is the AWGN at the n_{sc}-th subcarrier and $\circledast$ denotes the circular convolution operation. For ease of observation, in what follows we consider the signal produced after applying OFDM demodulation and removing the CP. Hence, the signal received at the n_{sc}-th subcarrier within the T_i-th STSK slot can be expressed as

$$\begin{aligned} \mathbf{R}_{T_i}(n_{sc}) = \mathbf{Z}(n_{sc})\hat{\mathbf{H}}(n_{sc})\mathbf{W}(n_{sc})\mathbf{X}_{T_i}(n_{sc}) \\ + \mathbf{V}(n_{sc}). \end{aligned} \tag{13}$$

Assuming that the channel remains constant during the STSK time interval T, after receiving all T OFDM symbols, the demapper shown in Figure 7 applies space-time de-mapping to each STSK symbol located at the n_{sc}-th subcarrier of all the received T OFDM symbols to a single received MS-STSK codeword and forward it to the MS-Decoder. For ease of notation, the subcarrier index n_{sc} is dropped in what follows, hence the n_{sc}-th received MS-STSK symbol can be expressed as

$$\mathbf{R} = \mathbf{Z}\hat{\mathbf{H}}\mathbf{W}\mathbf{X} + \mathbf{V}. \tag{14}$$

The assumption made here is that the AoD and AoA knowledge is available at both the transmitter and receiver, respectively, which implies that the optimal transmit and receive steering matrices $\mathbf{W}$ and $\mathbf{Z}$ are obtained at both ends. Therefore, the effective channel observed after applying the transmit and receive ABF is defined as

$$\mathbf{H} = \mathbf{Z}\hat{\mathbf{H}}\mathbf{W}, \tag{15}$$

where $\mathbf{H} \in \mathbb{C}^{N^r_{RF} \times N^t_{RF}}$. The received signal in (14) can now be expressed as

$$\mathbf{R} = \mathbf{H}\mathbf{X} + \mathbf{V}. \tag{16}$$

Following the philosophy of [18], the received signal in (16) can be reformulated to an SM equivalent model by applying the vectorial stacking operation, where the n_{sc}-th received MS-STSK symbol can be expressed as

$$\bar{\mathbf{R}} = \bar{\mathbf{H}}\mathcal{X}\mathcal{I}\mathbf{K} + \bar{\mathbf{V}}, \tag{17}$$

with

$$\bar{\mathbf{R}} = vec(\mathbf{R}) \in \mathbb{C}^{N^r_{RF}T \times 1}, \tag{18}$$

$$\bar{\mathbf{H}} = \mathbf{I} \otimes \mathbf{H} \in \mathbb{C}^{N^r_{RF}T \times N^t_{RF}T}, \tag{19}$$

$$\bar{\mathbf{V}} = vec(\mathbf{V}) \in \mathbb{C}^{N^r_{RF}T \times 1}, \tag{20}$$

$$\mathcal{X} = [vec(\tilde{A}_{1,1}) \dots vec(\tilde{A}_{q,n_{AC}}) \tag{21}$$

$$\dots vec(\tilde{A}_{q,N_{AC}})] \in \mathbb{C}^{N^t_{RF}T \times N_{AC}M_Q}, \tag{22}$$

given that $\mathbf{I}$ is a $(T \times T)$-element identity matrix, $\tilde{A}_{q,n_{AC}}$ is the MS-STSK dispersion matrix of the n_{AC}-th AC and $n_{AC} = 1, \dots, N_{AC}$.

The system in (17) is equivalent to an SM-MIMO system, where rather than activating a single antenna to transmit a single symbol as in SM, a combination of multiple antennas is activated in order to transmit a single STSK symbol, which is converted into an MS-STSK codeword after applying appropriate preprocessing. Furthermore, the matrix $\mathcal{I} \in \mathbb{C}^{N_{AC} M_Q \times M_Q}$ is used for selecting the activated AC and it is expressed as

$$\mathcal{I} = \mathcal{I}_{n_{AC}} = [\mathbf{0} \dots \underbrace{\mathbf{I}_{\mathbf{n_{AC}}}}_{n_{AC}-th\ element} \dots \mathbf{0}]^T, \tag{23}$$

where $\mathbf{I}_{\mathbf{n_{AC}}}$ is an $(M_Q \times M_Q)$-element identity matrix used for activating the n_{AC}-th AC. Correspondingly, the q-th dispersion matrix is activated by introducing a single modulated symbol s_l in the q-th position of $\mathbf{K}$, where $\mathbf{K} \in \mathbb{C}^{M_Q \times 1}$ and it is defined as

$$\mathbf{K} = [\underbrace{0, \dots, 0}_{q-1}, s_l, \underbrace{0, \dots, 0}_{M_Q - q}]^T. \tag{24}$$

Hence, (17) can be reformulated as

$$\begin{aligned} \bar{\mathbf{Y}} = & \begin{bmatrix} \mathbf{H} & \cdots & \mathbf{0} \\ \vdots & \ddots & \vdots \\ \mathbf{0} & \cdots & \mathbf{H} \end{bmatrix} \\ & \cdot \begin{bmatrix} \cdots & \begin{bmatrix} \hat{\mathbf{A}}_{1,n_{AC}} & \cdots & \hat{\mathbf{A}}_{Q,n_{AC}} \end{bmatrix} & \cdots \end{bmatrix} \\ & \cdot \begin{bmatrix} \mathbf{0} \\ \vdots \\ \mathbf{I}_{\mathbf{n_{AC}}} \\ \vdots \\ \mathbf{0} \end{bmatrix} \\ & \cdot \begin{bmatrix} 0 \\ \vdots \\ s_l \\ \vdots \\ 0 \end{bmatrix} + \bar{\mathbf{V}}, \end{aligned} \tag{25}$$

where $\hat{\mathbf{A}}_{q,n_{AC}} = vec(\tilde{\mathbf{A}}_{q,n_{AC}}) \in \mathbb{C}^{N_{RF}^t T \times 1}$.

The MS-STSK dispersion matrix $\tilde{A}_{q,n_{AC}} \in \mathbb{C}^{N_{RF}^t \times T}$ is the modified version of the simplified STSK dispersion matrix A_q of [18]. It can be defined as the counterpart of the dispersion matrix A_q with zeros values representing the inactive antennas, yielding

$$\tilde{A}_{q,n_{AC}} = \begin{bmatrix} \mathbf{0} \\ \vdots \\ A_{q,m} \\ \vdots \\ \mathbf{0} \end{bmatrix} . e^{j(\theta_{n_{AC}})}, \tag{26}$$

where $A_{q,m} \in \mathbb{C}^{1 \times T}$ is the m-th row of A_q and $m = 1, \dots, M$.

With the aid of an ML detector, the receiver becomes capable of obtaining $\hat{q}$, $\hat{l}$ and $\hat{n}_{AC}$, namely the estimates of the dispersion matrix index q, the modulated symbol index l and the AC index n_{AC}, respectively, as

$$< \hat{q},\ \hat{l},\ \hat{n}_{AC} > = \arg \min_{q,l,n_{AC}} \left\| \bar{\mathbf{R}} - \bar{\mathbf{H}} \mathcal{X} \mathcal{I}_{n_{AC}} \mathbf{K}_{q,l} \right\|^2. \tag{27}$$

However, owing to the fact that hard-decision decoding is employed at the receiver, the detection complexity order can be further reduced from $\mathcal{O}(M_Q M_c N_{AC})$ to $\mathcal{O}(M_Q N_{AC})$, while retaining the optimality of detection with the aid of the Hard-Limiter ML (HL-ML) detection employed in [18], yielding

$$\begin{aligned} < \hat{q},\ \hat{n}_{AC} > = \arg \min_{q,n_{AC}} (& \left| \hat{\mathbf{r}}_{n_{AC},q} - \hat{s}_l \right|^2 \\ & - \left| \hat{\mathbf{r}}_{n_{AC},q} \right|^2) \left\| \mathbf{h}_{n_{AC},q} \right\|^2, \end{aligned} \tag{28}$$

where $\mathbf{H}_{\mathbf{n_{AC}}} = [\mathbf{h}_{n_{AC},1} \dots \mathbf{h}_{n_{AC},M_Q}] \in \mathbb{C}^{N_r T \times M_Q}$, $\hat{s}_l$ is the estimated M_c-QAM/PSK symbol and $\hat{\mathbf{r}}_{n_{AC},q}$ is the equalized received symbol denoted by

$$\hat{\mathbf{r}}_{n_{AC},q} = \frac{\mathbf{h}_{n_{AC},q}^H \bar{\mathbf{R}}}{\left\| \mathbf{h}_{n_{AC},q} \right\|^2}. \tag{29}$$

C. MS-STSK PHASE ROTATION

The phase rotation $\theta_{n_{AC}}$ in (4) is applied to each STSK codeword transmitted over the n_{AC}-th AC in order to overcome the correlation between the specific STSK codewords sharing some TAAs [18]. Again, this correlation is introduced by transmitting different STSK codewords over the same AC and it was shown in [18] that this correlation can lead to a performance degradation. For the sake of obtaining the best rotation phase for each M_c-QAM/PSK modulation, we applied brute-force ML detection for several OFDM-MS-STSK systems associated with different modulation schemes. All simulations were carried out at high SNR with an incremental step of 1° for each iteration of $\Delta\theta$ from 0° to 360°, where $\Delta\theta = \theta_{n_{AC}+1} - \theta_{n_{AC}}$ is the phase difference between two AC rotations. Furthermore, each simulation was carried out by generating 25,000 bits over 50 iterations.

Four distinct scenarios were considered for determining the best values of $\Delta\theta$ as follows. OFDM-MS-STSK system with $N_{RF}^t = 4$ and STSK(2,2,2,4,BPSK) encoder, $N_{RF}^t = 5$ and STSK(2,2,2,4,8PSK) encoder, $N_{RF}^t = 4$ and STSK(2,2,2,4,4QAM) encoder and $N_{RF}^t = 4$ and STSK(2,2,2,4,16QAM) encoder. The number of TAAs was set to $N_{RF}^t = 4$, the number of RAAs to $N_{RF}^r = 2$, the number of STSK spaces to $M = 2$ and $T = 2$ time slots were used for all systems the considered in order to exclusively evaluate the impact of the modulation scheme employed on the choice of the phase-shift $\theta_{n_{AC}}$. The BER performance versus the phase-shift angle of the OFDM-MS-STSK(4, 2, 2, 2, 4,4QAM) system associated with the SAC configuration and transmitting over the mmWave channel at SNR = 19 dB[2] is shown in Figure 8. This figure shows that the phase-shift has an impact on the performance of the system, where for instance Figure 8 shows that the minimum BER of 1.6e-05 was achieved at

[2]The SNR value is chosen such that the considered system achieves a BER of $\leq 10^{-4}$.

TABLE 4. Phase rotation difference applied to different ACs with BPSK, 8PSK, 4QAM, and 16QAM modulation techniques.

M_c	Modulation	$\Delta\theta$(degree)
2	PSK	42°/86°12°/100°
8	PSK	85°, 111°, 129°, 305°, 349°
4	QAM	288°
16	QAM	35°, 124°

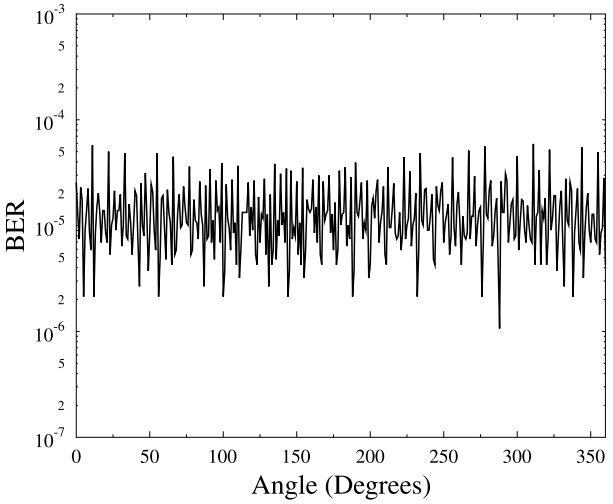

FIGURE 8. BER versus phase-shift performance of OFDM-MS-STSK (4, 2, 2, 2, 4,4QAM) at SNR=19 dB with an incremental step of 1° for each iteration of $\Delta\theta$ from 0° to 360°.

$\Delta\theta = 288°$ for the OFDM-MS-STSK(4, 2, 2, 2, 4, 4QAM) system at SNR = 19 dB, while the maximum BER of 5.92e-05 was achieved at $\Delta\theta = 311°$ at the same SNR. Similarly, the best phase-shift values[3] for the OFDM-MS-STSK(4, 2, 2, 2, 4,BPSK), OFDM-MS-STSK(4, 2, 2, 2, 4,4QAM), OFDM-MS-STSK(4, 2, 2, 2, 4,8PSK) and OFDM-MS-STSK(4, 2, 2, 2, 4,16QAM) systems were obtained from Monte Carlo simulations, where a summary of their values is provided in Table 4. Furthermore, the third row of Table 4 shows the best phase-shift values for the OFDM-MS-STSK(4, 2, 2, 2, 4, 8PSK) system at SNR = 21 dB, where zero errors were detected over 50 iterations at $\Delta\theta = 85°, 111°, 129°, 305°$ and 349°. The attainable throughput of the OFDM-MS-STSK system is evaluated in the following subsection.

D. OFDM-MS-STSK THROUGHPUT

In the OFDM-MS-STSK scheme, an OFDM symbol associated with N_{sc} MS-STSK codewords carries $(N_{sc} + N_{cp})$ symbols, where N_{cp} is the length of the CP. Consequently, the overall throughput of the system is affected by the length of CP. Given that each subcarrier carries $\log_2(M_q M_c)$ bits over the interval T by the STSK codeword and $\log_2(N_{AC})$ bits by the AC index, the system's throughput is defined as

$$R_{MS-STSK} = \frac{\log_2(M_q M_c N_{AC})}{\left(1 + \frac{N_{cp}}{N_{sc}}\right)} \text{ (bps)}, \tag{30}$$

$$= \underbrace{\frac{\log_2(M_q M_c)}{\left(1 + \frac{N_{cp}}{N_{sc}}\right)}}_{R_{STSK}} + \underbrace{\frac{\log_2(N_{AC})}{\left(1 + \frac{N_{cp}}{N_{sc}}\right)}}_{R_{AC}}, \tag{31}$$

where $R_{MS-STSK}$ represents the throughput of the entire MS-STSK OFDM symbol in bits per symbol, R_{STSK} is the throughput of the STSK part of the OFDM-MS-STSK, R_{AC} is the rate of extra bits conveyed by the AC index and bps short for bits per symbol.

At mmWaves, the delay-spread is of an order of nanoseconds [35], [43]. In principle, channels associated with short delay spreads are preferable over large delay spread channels, since they impose zero ISI due to their non-dispersive nature. However, owing to their huge bandwidths, operating at mmWave frequency bands requires high sampling rates, where for instance a minimum of 1 GHz sampling rate is required for using a chunk of 500 MHz bandwidth at the 28 GHz frequency band. Thereby, even a few nanoseconds of multipath delay spread becomes non-negligible at say one nanosecond sampling time. Hence, a long CP is necessary for overcoming the effect of the time dispersive wideband mmWave channel. Nevertheless, the large bandwidths of mmWave channels allow a huge number of subcarriers compared to the sub-3 GHz frequency bands, which reduces the denominator of (30) to $\left(1 + \frac{N_{cp}}{N_{sc}}\right) \lessapprox 1$. Hence, finally we arrive at

$$[R_{MS-STSK}]_{\frac{N_{cp}}{N_{sc}} \approx 0} \rightarrow \log_2(M_q M_c N_{AC})\,(bps). \tag{32}$$

The OFDM-MS-STSK throughput per OFDM symbol associated with a CP length of $N_{cp} = 100$ versus the number of subcarriers N_{sc} compared to the MS-STSK scheme's throughput [18] is illustrated in Figure 9. The figure shows that as the number of subcarriers exceeds 1024 subcarriers, i.e. $N_{sc} \geq 1024$, the OFDM-aided scheme attains 90% of the maximum achievable MS-STSK throughput, which we refer to as the normalized throughput ∂_{MS} is defined by the ratio of the attainable throughput of the MS-STSK OFDM-aided scheme over that of the classical MS-STSK scheme's throughput in [18], which can be expressed as

$$\partial_{MS} = \frac{R_{MS-STSK}}{[R_{MS-STSK}]_{\frac{N_{cp}}{N_{sc}} \approx 0}} \tag{33}$$

$$= \frac{\left(\frac{\log_2(Q \cdot \mathcal{L} \cdot N_{AC})}{\left(1 + \frac{N_{cp}}{N_{sc}}\right)}\right)}{\log_2(Q \cdot \mathcal{L} \cdot N_{AC})} \tag{34}$$

$$= \frac{1}{\left(1 + \frac{N_{cp}}{N_{sc}}\right)} \tag{35}$$

$$= \frac{N_{sc}}{(N_{sc} + N_{cp})}. \tag{36}$$

[3]Best phase-shift corresponds to the phase-shift resulting in the lowest BER.

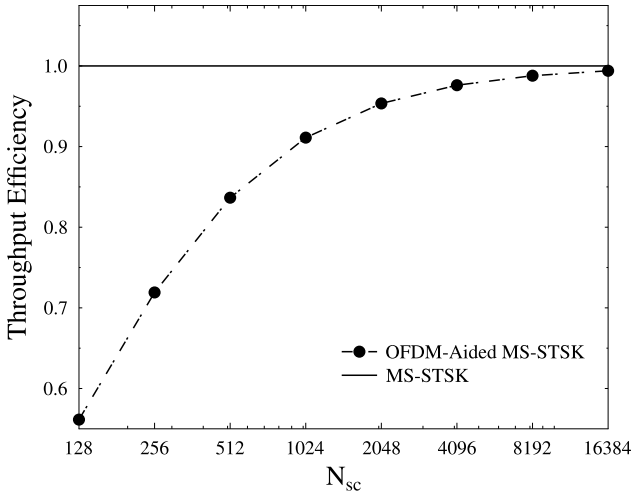

FIGURE 9. Efficiency of the OFDM-MS-STSK with $N_{cp} = 100$ throughput compared to the conventional STSK throughput versus the number of subcarriers N_{sc}.

Furthermore, dividing the bandwidth into 8192 subcarriers allows the OFDM-MS-STSK scheme to achieve a throughput efficiency of nearly 98%.

The number of extra bits carried by the AC index R_{AC} versus the number of TAAs N_{RF}^{t} as a function of M associated with $N_{sc} = 8192$ subcarriers and $N_{cp} = 100$ is shown in Figure 10. The number of TAAs spans between $M \leq N_{RF}^{t} \leq 64$, where $M = 2, 4, 6, 8, 10, \ldots, 32$. Based on (2), as the number of TAAs increases with respect to the value of M of the STSK encoder, the number of ACs increases, which means that more bits are conveyed over the activated AC index. However, having more ACs widens the search space of the detector, hence increasing its complexity order. Furthermore, as shown in Figure 10, the OFDM-aided STSK schemes proposed in [32], [44]–[46] constitute special cases of the OFDM-aided MS-STSK, namely when $N_{RF}^{t} = M$.

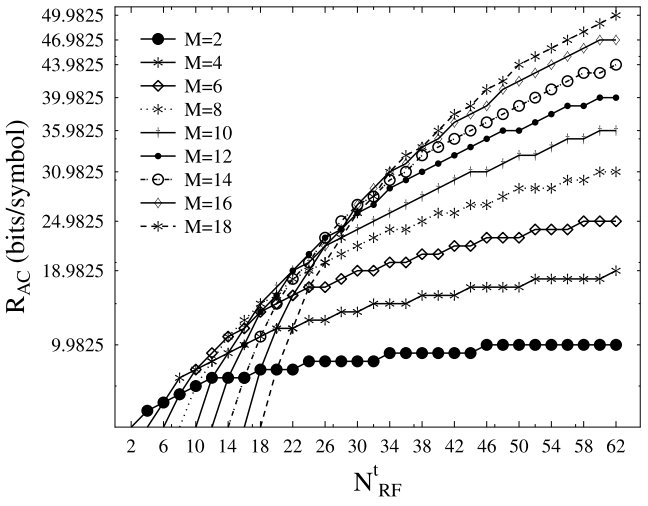

FIGURE 10. Achievable number of bits characterizing the AC indexes, R_{AC}, per subcarrier associated with $N_{sc} = 8192$ subcarriers, and $N_{cp} = 100$.

TABLE 5. Main simulation parameters for the OFDM-MS-STSK over the 28 GHz mmWave channel. RMS DS*: Root Mean Square Delay Spread. AoA & AoD AS**= AoA & AoD Angular Spread.

Parameters	Values
Carrier Frequency	28 GHz
Bandwidth	500 MHz
P_t	30 dB
G_{Rx}	24 dBi
G_{Tx}	24 dBi
Transmitter	MS-STSK
N_{sc}	8192
N_{cp}	100
Distance	<200 m
N_{cl}	Poiss($\mu = 3.4$, $\sigma = 2.1$)
$N_p(n_c)$	Exp($\mu = 66.3$, $\sigma = 68.0$)
RMS DS*	Exp($\mu = 13.4$, $\sigma = 11.5$)
AoA & AoD AS**	Exp($\mu = 34.6$, $\sigma = 27.8$)
$\bar{\varphi}^{Rx}$and $\bar{\varphi}^{Tx}$	U(0, 360)

E. PERFORMANCE RESULTS

In this section, we characterize the performance of our OFDM-MS-STSK system for transmission over the 28 GHz wideband channel using the Monte-Carlo technique. The simulation parameters are summarized in Table 5 based on the channel measurements in [34], [39].

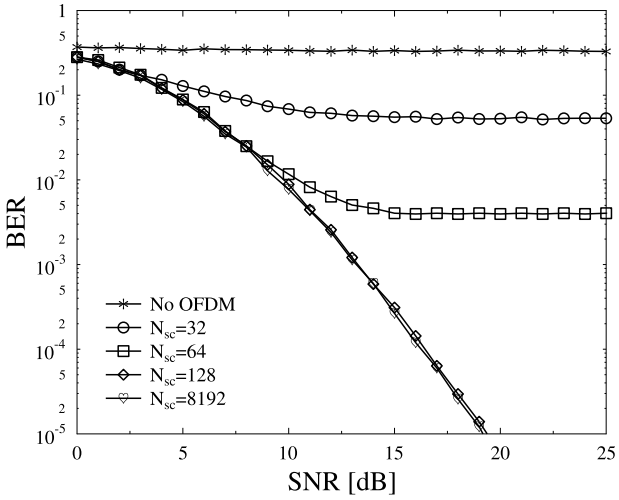

FIGURE 11. BER performance of an OFDM-MS-STSK with $N_{RF}^{t} = 4$ TAAs with single AE, STSK(2, 2, 2, 4, 4) encoder, and $\Delta\theta = 7°$.

The BER performance of the OFDM-MS-STSK system transmitting over the mmWave channel having different number of subcarriers is shown in Figure 11 for an MS-STSK transmitter associated with $N_{RF}^{t} = 4$ single AE TAAs equipped with an STSK(2,2,2,4,4QAM) encoder. Furthermore, based on the values presented in Table 4, the phase rotation difference between each of the $N_{AC} = 4$ ACs is $\Delta\theta = 288°$. Moreover, the receiver employed applies ML detection to each received MS-STSK codeword at each subcarrier.

When a single-carrier system is used, the performance of the conventional MS-STSK [18] communicating over the mmWave channel has an error floor, as shown by the curve with the (*) marker in Figure 11. Furthermore, observe that the number of subcarriers is the huge 500 MHz bandwidth affects the performance of the system. Explicitly, subdividing it into a small number of subcarriers produces an error floor at $N_{sc} = 32$ and $N_{sc} = 64$ due to the wideband nature of the sub-bands. On the other hand, using $N_{sc} = 128$ subcarriers is sufficient in the 28 GHz band for a bandwidth of 500 MHz. Furthermore, the performance of the system remains unaffected by dispersion at $N_{sc} = 8192$ subcarriers, which facilitates more efficient transmission at a given CP length owing to the reduced overhead.

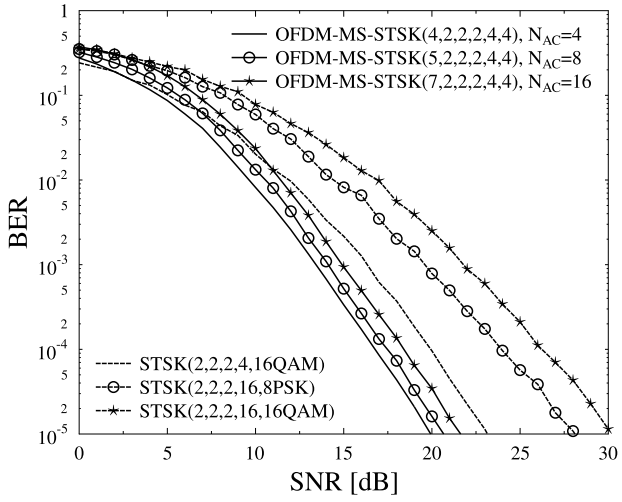

FIGURE 12. BER performance of the OFDM-MS-STSK system equipped with $N_{RF}^t = 4$, $N_{RF}^t = 5$, and $N_{RF}^t = 7$ TAAs each with a single AE and STSK(2,2,2,2,4QAM) encoder achieving a throughput of 6, 7, and 8 bps, respectively, compared to their OFDM-STSK equivalent systems with STSK(2,2,2,4,16QAM), STSK(2,2,2,16,8PSK), and STSK(2,2,2,16,16QAM) encoders, respectively, over mmWave channel. Based on Table 4, the phase rotation differences used for 8PSK, 4QAM, and 16QAM are $\Delta\theta_{AC} = 85°$, 288°, and 35°.

The simulation results recorded for our proposed OFDM-MS-STSK system in conjunction with different system configurations compared to the corresponding OFDM-STSK at same throughput is shown in Figure 12. The HL-ML detector of Section II-B is employed, which matches the optimal ML performance of [18]. Figure 12 shows the BER performance of an OFDM-MS-STSK system equipped with $N_{RF}^t = 4$, $N_{RF}^t = 5$ and $N_{RF}^t = 7$ TAAs, each with a single AE and STSK(2,2,2,2,4QAM) encoder achieving a throughput of 6, 7 and 8 bps, respectively. The system associated with these configurations is compared to an equivalent OFDM-STSK system relying on STSK(2,2,2,4,16QAM), STSK(2,2,2,16,8PSK) and STSK(2,2,2,16,16QAM) encoders, respectively, for transmission over the mmWave channel [19] in conjunction with $N_{sc} = 8192$ subcarriers. Furthermore, based on Table 4, the phase rotation differences used for 8PSK, 4QAM and 16QAM are $\Delta\theta_{AC} = 85°$, 288° and 35°, respectively. The proposed OFDM-MS-STSK system outperforms the conventional STSK scheme by nearly 5 dB, 10 dB and 13 dB at a throughput of 6, 7 and 8 bits, respectively.

When employing the optimal ML detector at all receivers, the complexity order of all OFDM-MS-STSK detectors used in all cases is equivalent to the corresponding OFDM-STSK detectors' complexity order. For example, the complexity order of the OFDM-MS-STSK system having $N_{RF}^t = 7$ TAAs and STSK(2,2,2,4,4) is $\mathcal{O}\left(N_{AC} \times M_Q \times M_c\right) = \mathcal{O}\left(8 \times 4 \times 4\right)$, which is equal to its equivalent throughput OFDM-STSK(2,2,2,16,8) system of $\mathcal{O}\left(M_Q \times M_c\right) = \mathcal{O}\left(8 \times 16\right)$. Furthermore, the complexity order of the OFDM-MS-STSK system having $N_{RF}^t = 4$ and STSK(2,2,2,4,4) is $\mathcal{O}\left(4 \times 4 \times 4\right)$, which is equal to its equivalent throughput OFDM-STSK(2,2,2,4,16) system of $\mathcal{O}\left(4 \times 16\right)$.

Similarly, when employing the HL-ML detector, which was used in the simulations, the complexity order of both the OFDM-MS-STSK detector, as well as of the equivalent OFDM-STSK detector is reduced by M_c. For example, the complexity order of the OFDM-MS-STSK system associated with $N_{RF}^t = 7$ and STSK(2,2,2,4,4) is $\mathcal{O}\left(N_{AC} \times M_Q\right) = \mathcal{O}\left(8 \times 4\right)$, while the equivalent-throughput system OFDM-STSK(2,2,2,16,8) has a complexity order of $\mathcal{O}(M_Q) = \mathcal{O}(16)$, which is lower than that of the former. This reduced complexity order is achieved as a result of the system configuration choice, not as a benefit of the MS-STSK technique itself, where changing the MS-STSK encoder's settings is capable of further reducing the complexity order at a given throughput.

By employing multiple AEs at each TAA and RAA, the system is capable of acquiring extra SNR gain with the aid of analogue beamforming. The effect of adding extra AEs to each AA by invoking optimal analogue beamforming is shown in Figure 13, which portrays the BER performance of an OFDM-MS-STSK system associated with an $N_{RF}^t = 7$ and STSK(2,2,2,4,4QAM) encoder equipped by different numbers N_{AA}^t and N_{AA}^r of AEs.

Given that the optimal analogue beamforming gain is equal to $+10\log(N_{AA}^t N_{AA}^r)$, it is shown in Figure 13 that employing $(N_{AA}^t = 2, N_{AA}^r = 1)$, $(N_{AA}^t = 2, N_{AA}^r = 2)$, $(N_{AA}^t = 4, N_{AA}^r = 2)$ and $(N_{AA}^t = 10, N_{AA}^r = 2)$ lends about 3 dB, 6 dB, 9 dB and 13 dB SNR gain to the system, which are of great importance at mmWaves in order to overcome the high path loss.

III. MULTI-SPACE-FREQUENCY STSK OVER mmWAVES

In this section, we introduce our novel Multi-Space-Frequency STSK (MSF-STSK) system. As described in Section II, the wideband mmWave channel may be partitioned into sub-bands in order to employ OFDM in the proposed OFDM-MS-STSK system. Additionally, as in Section II, the number of ACs used can be lower than the total number of ACs, where N_{AC} is limited to integer powers of 2, so that 2^k binary sets can be generated. Hence, the extra number of ACs may be utilized in order to convey extra

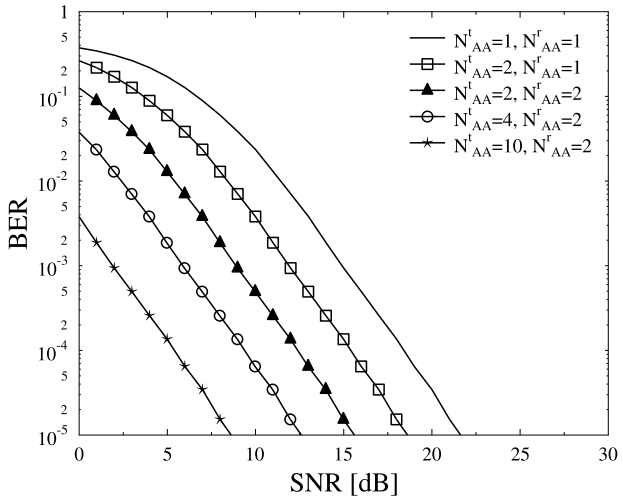

FIGURE 13. BER performance of the OFDM-MS-STSK(7, 2, 2, 2, 4, 4QAM) system equipped with TAAs and RAAs having multiple sizes.

information over the subcarrier index domain in a similar way to the technique used in the Generalized Space-Frequency Index Modulation (GSFIM) [30].

In GSFIM, the bits are encoded over both the TAE index and the subcarrier index for the sake of enhancing the achievable throughput [30]. In our MSF-STSK system, information is transmitted over the following three components: The first two parts are the STSK codeword and the AC index, similar to the MS-STSK scheme, while the third component is the Frequency Index (FI) of the subcarriers with a block of subcarriers where the extra ACs are detected, as described next.

A. MSF-STSK TRANSMITTER

The proposed MSF-STSK transmitter's block diagram is identical to that of the OFDM-MS-STSK scheme shown in Figure 4. However, the MS-digital encoder is replaced by an MSF-digital encoder, which only differ at the digital encoding level. Hence, the OFDM-MS-STSK and MSF-STSK schemes are digitally interchangeable.

Given that the MSF-STSK transmitter is equipped with N_{RF}^t TAAs, the MSF-STSK encoder is fed with a block of $B_{MSF-STSK}$ bits, which divides the input bits into B_{STSK},[4] B_{ASU}[5] and B_{FI}[6] bits with the aid of the serial-to-parallel (S/P) converter in order to encode the STSK codeword as well as to select the MS-STSK subcarrier AC and the FI of the subcarriers block,[7] respectively. The N_{sc} subcarriers are partitioned into blocks of subcarriers each containing $N_B = 2^{\bar{q}}$ subcarriers, where we have

$$B_{FI} = \lfloor \log_2 (N_{FI} N_B) \rfloor, \tag{37}$$

[4] B_{STSK} bits are used to select one out of Q STSK codewords.

[5] B_{ASU} bits are used to activate one out of N_{AC} antenna combinations.

[6] B_{FI} bits are used to select the frequency index of the subcarriers block of size N_B.

[7] A block of subcarriers is described as a set of consecutive N_B subcarriers, which are used to encode the frequency index.

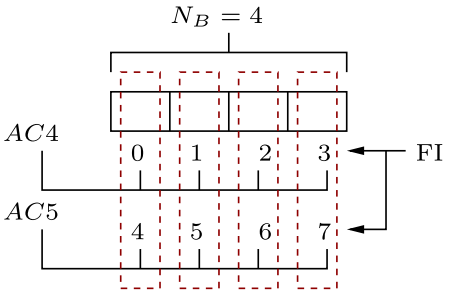

FIGURE 14. 4-th AC describes the first four FI realizations FI = 0, 1, 2, or 3 when located at $n_B = 1, 2, 3,$ or 4, while the 5-th AC describes the next four FI realizations FI = 4, 5, 6, or 7 when located at $n_B = 1, 2, 3,$ or 4.

TABLE 6. MSF mapping table of a transmitter equipped with $M = 2$ and $N_{RF}^t = 4$, where AC = 0, 1, 2 and 3 are dedicated for the MS-STSK part and AC=4, and 5 are dedicated for frequency indexing.

AC	TAA Combination
0	$\{TAA_1, TAA_2\}$
1	$\{TAA_1, TAA_3\}$
2	$\{TAA_1, TAA_4\}$
3	$\{TAA_2, TAA_3\}$
4	$\{TAA_2, TAA_4\}$
5	$\{TAA_3, TAA_4\}$

and $N_{FI} = 2^{\bar{p}}$ is the number of ACs dedicated to FI encoding with $n_B = 1, \ldots, N_B$. For ease of implementation, consider an MSF-STSK system with $N_{RF}^t = 4$ TAAs, $M = 2$ STSK spaces and a block size of $N_B = 4$. Here, the total number of ACs is 6, of which the MS-STSK scheme utilizes only $N_{AC} = 4$. Hence, in MSF-STSK, the extra $N_{FI} = 2$ ACs may be used for encoding the FI, which leads to $B_{FI} = \lfloor \log_2 (2 \times 4) \rfloor = 3$ and $2^3 = 8$ FI realizations. As shown in Table 6, the first four combinations 0, 1, 2 and 3 are used for mapping a symbol to a specific subcarrier based on the MS-STSK scheme, while the remaining two ACs, namely 4 and 5 are used for applying the block frequency indexing, or the FI encoding. As shown in Figure 14, the 4-th AC, describes the first four FI realizations of FI = 0, 1, 2 or 3 when located at $n_B = 1, 2, 3$ or 4, while the 5-th AC describes the next four FI realizations FI = 4, 5, 6 or 7 when located at $n_B = 1, 2, 3$ or 4. In other words, the location of each of the N_{FI} ACs, given by the 4-th and 5-th AC in this example, in a block of N_B subcarriers, given by $N_B = 4$ subcarriers, defines the frequency index of the each subcarrier block.

For further illustration, let us consider three frequency blocks of size $N_B = 4$ subcarriers encoded using the MSF-encoder. Assuming that three input bit streams of $L1$, $L2$ and $L3$ are defined as

$$L1 = \{\underbrace{110}_{FI} - \underbrace{00}_{MS}\ \underbrace{0\cdots00}_{STSK}$$

$$- \underbrace{01}_{MS}\underbrace{0\cdots00}_{STSK} - \underbrace{0\cdots00}_{STSK} - \underbrace{11}_{MS}\underbrace{0\cdots00}_{STSK}\}, \quad (38)$$

$$L2 = \{\underbrace{000}_{FI} - \underbrace{0\cdots00}_{STSK} - \underbrace{00}_{MS}\underbrace{0\cdots00}_{STSK} - \underbrace{11}_{MS}\underbrace{0\cdots00}_{STSK} - \underbrace{10}_{MS}\underbrace{0\cdots00}_{STSK}\}, \quad (39)$$

$$L3 = \{\underbrace{011}_{FI} - \underbrace{10}_{MS}\underbrace{0\cdots00}_{STSK} - \underbrace{11}_{MS}\underbrace{0\cdots00}_{STSK} - \underbrace{01}_{MS}\underbrace{0\cdots00}_{STSK} - \underbrace{0\cdots00}_{STSK}\}, \quad (40)$$

where the notation $\underbrace{0\cdots00}_{STSK}$ is used for describing a random bit sequence employed for generating the STSK codeword.

By referring to Figure 15, $L1$ is encoded into the first N_B subcarriers block as follows. The first 3 bits describe the FI encoding, where 110 refers to the 6-th FI realisation, which can be encoded using the 5-th AC at $n_B = 3$. The other 3 subcarriers are encoded based on the conventional MS-STSK scheme, where ACs 0, 1 and 3 are mapped to $n_B = 1$, $n_B = 2$ and $n_B = 4$, respectively. Furthermore, $L2$ is encoded into the next N_B subcarrier block as follows. The first 000 bits refer to the 1-st FI realization, which can be encoded using the 4-th AC at $n_B = 1$. The other 3 subcarriers at $n_B = 2$, $n_B = 3$ and $n_B = 4$ are mapped to ACs 0, 3 and 2, respectively. Lastly, $L3$ is encoded into the third N_B subcarrier block as follows. The first 011 bits refer to the 3-rd FI realization, which can be encoded using the 4-th AC at $n_B = 4$, while ACs 2, 3 and 1 are mapped to $n_B = 1$, $n_B = 2$ and $n_B = 3$, respectively.

Note that in other TAA-to-M configurations, where the number of extra ACs exceeds the required N_{FI} for FI encoding, it is recommended to choose N_{FI} out of the available extra ACs. For example, consider an MSF-STSK system equipped with $N_{RF}^t = 6$ RF chains and associated with an STSK encoder having $M = 2$. The total number of ACs is equal to 15, which means that $N_{AC} = 8$ ACs are used for MS-STSK encoding, while $N_{FI} = 2$ or 4 ACs out of the extra 7 ACs may be assigned for FI encoding. The procedure of constructing the OFDM symbol and the switching process in the MSF-STSK encoding is identical to the OFDM-MS-STSK scheme presented in Section II-A. In the next subsection, we introduce the MSF-STSK receiver.

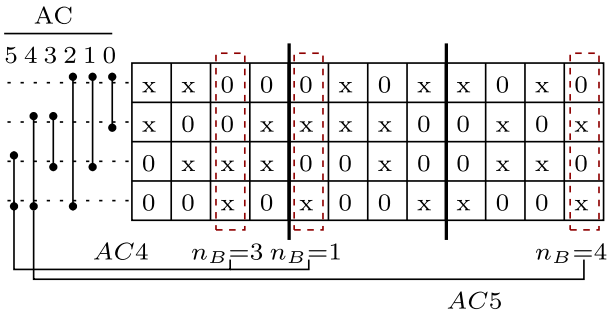

FIGURE 15. MSF-STSK encoding of $L1$, $L2$, and $L3$ in (38), (39), and (40), respectively.

B. MSF-STSK RECEIVER

Similarly, the receiver block diagram of the MSF-STSK system is equivalent to that of the OFDM-MS-STSK receiver shown in Figure 7, where the MS-STSK digital decoder is replaced by an MSF-STSK decoder. Assuming the same receiver configurations as in Section II-B, the detection procedure of the MSF-STSK decoder is applied on a per subcarrier block basis.

Consider that the N_{sc} subcarriers are subdivided into N_{SB} blocks, each having N_B subcarriers and recalling (16), the received signal after applying receive beamforming and OFDM demodulation at the n_B-th subcarrier in the n_{sb}-th block is modeled as

$$\mathbf{R}_{n_B}^{n_{sb}} = \mathbf{H}_{n_B}^{n_{sb}} \mathbf{X}_{n_B}^{n_{sb}} + \mathbf{V}_{n_B}^{n_{sb}}, \quad (41)$$

where $\mathbf{R}_{n_B}^{n_{sb}}$, $\mathbf{H}_{n_B}^{n_{sb}}$, $\mathbf{X}_{n_B}^{n_{sb}}$ and $\mathbf{V}_{n_B}^{n_{sb}}$ are the received signal, the mmWave channel, the received symbol and the noise at the n_B-th subcarrier in the n_{sb}-th block, with $n_{sb} = 1, \ldots, N_{SB}$. Then, the detection of each block is carried out in two stages with the aid of an optimal ML detector. The first stage detects the block's FI by obtaining $(\hat{n}_{FI}, \hat{n}_B)$, which represents the estimates of the AC used $n_{FI} = 1, \ldots, N_{FI}$ and the subcarrier index n_B, while $\hat{q}_{FI}$ and $\hat{l}_{FI}$ are the estimates of the dispersion matrix and of the QAM/PSK symbol indices of the $(\hat{n}_{FI}, \hat{n}_B)$ STSK symbol, yielding

$$< \hat{q}_{FI}, \hat{l}_{FI}, (\hat{n}_{FI}, \hat{n}_B) > = \arg \min_{n_B, q, l, n_{FI}} \left\| \bar{\mathbf{R}}_{n_B}^{n_{sb}} - \bar{\mathbf{H}} \mathcal{X} \mathcal{I}_{n_{FI}} \mathbf{K}_{q,l} \right\|^2, \quad (42)$$

where $n_B = 1, \ldots, N_B$, $\bar{\mathbf{R}}_{n_B}^{n_{sb}} = vec(\mathbf{R}_{n_B}^{n_{sb}})$ and $\mathcal{I}_{n_{FI}} = [\mathbf{0} \ldots \mathbf{I}_{n_{FI}} \ldots \mathbf{0}]^T \in \mathbb{C}^{N_{FI} M_Q \times M_Q}$, where an $(M_Q \times M_Q)$-element identity matrix $\mathbf{I}_{n_{FI}}$ is used to activate the n_{FI}-th AC.

After determining the FI index of the n_{sb}-th block, the second stage is activated for detecting MS-STSK symbols at the other subcarriers as

$$< \hat{q}_{\bar{n}_B}, \hat{l}_{\bar{n}_B}, \hat{n}_{AC} > = \arg \min_{q, l, n_{AC}} \left\| \bar{\mathbf{R}}_{\bar{n}_B}^{n_{sb}} - \bar{\mathbf{H}} \mathcal{X} \mathcal{I}_{n_{AC}} \mathbf{K}_{q,l} \right\|^2, \quad (43)$$

where $\bar{n}_B = 1, \ldots, n_{FI}-1,\ n_{FI}+1, \ldots N_B$ and $\hat{q}_{\bar{n}_B}$, $\hat{l}_{\bar{n}_B}$ and $\hat{n}_{AC}$ represent the estimates of the dispersion matrix index, of the modulated symbol index and of the AC index n_{AC} at the $\bar{n}_B$-th subcarrier in the n_{sb}-th block, respectively.

However, owing to the fact that each subcarrier in the MSF-STSK symbol is equivalent to the OFDM MS-STSK symbol, the reduced-complexity HL-ML optimal detector of [18] and defined in equation (28) can be invoked for further reducing the complexity order of the MSF-STSK detector. Hence, the stage one decoding can be formulated as

$$< \hat{q}_{n_B},\ \hat{n}_{FI} > = \arg \min_{q,n_{AC}} \left(\left| \hat{\mathbf{r}}_{n_B,q} - \hat{s}_{l_{n_B}} \right|^2 - \left| \hat{\mathbf{r}}_{n_B,q} \right|^2 \right) \left\| \mathbf{h}_{n_{FI},q} \right\|^2, \quad (44)$$

where $\hat{s}_{l_{n_B}}$ is the M_c-QAM/PSK symbol estimated at the n_B-th subcarrier in the n_{sb} block and $\hat{\mathbf{r}}_{n_B,q}$ is the equalized received symbol denoted by

$$\hat{\mathbf{r}}_{n_B,q} = \frac{\mathbf{h}^H_{n_B,q} \mathbf{R}^{\bar{n}_{sb}}_{n_B}}{\left\| \mathbf{h}_{n_B,q} \right\|^2}. \quad (45)$$

By contrast, the stage two detection at the $\bar{n}_B$ subcarrier can be translated into

$$< \hat{q}_{\bar{n}_B},\ \hat{n}_{AC} > = \arg \min_{q,n_{AC}} \left(\left| \hat{\mathbf{r}}_{n_{AC},q} - \hat{s}_{l_{\bar{n}_B}} \right|^2 - \left| \hat{\mathbf{r}}_{n_{AC},q} \right|^2 \right) \left\| \mathbf{h}_{n_{AC},q} \right\|^2, \quad (46)$$

where $\hat{s}_{l_{\bar{n}_B}}$ is the M_c-QAM/PSK symbol estimated at the $\bar{n}_B$-th subcarrier in the n_{sb} block.

C. MSF-STSK THROUGHPUT

The main advantage of MSF-STSK over the OFDM-MS-STSK scheme is its enhanced throughput, where encoding the FI of each block of subcarriers adds extra information to the transmitted symbol. The bit rate per subcarrier of MSF-STSK is defined as

$$R_{n_s} = \frac{\log_2(M_q M_c)}{N_B} \{(N_B - 1)\log_2(N_{AC}) + \log_2(N_B N_{FI})\} \text{ (bit/subcarrier)}, \quad (47)$$

while the bit rate per block as

$$R_{n_{bs}} = \log_2(M_q M_c)\{(N_B - 1)\log_2(N_{AC}) + \log_2(N_B N_{FI})\} \text{ (bit/block)}, \quad (48)$$

whereas the symbol rate of MSF-STSK, while taking into consideration the CP length is defined as

$$R_{MSF-STSK} = \frac{R_{n_{bs}}}{N_B \left(N_{sc} + N_{cp}\right)} \text{ (bps)}. \quad (49)$$

For the sake of achieving a higher throughput in MSF-STSK than MS-STSK, the size of the block should be constrained by the condition of

$$\log_2(N_B N_{FI}) > \log_2(N_{AC}). \quad (50)$$

The specific choice of the block size N_B is crucial in order to achieve the optimal system throughput. At a given number of antenna combinations for N_{AC} and N_B, the total number of bits transmitted per block using the MSF-STSK scheme reaches its maximum, when $\triangle\tilde{R}$ reaches its maximum value, given that

$$\triangle\tilde{R} = \tilde{R}_{MSF} - \tilde{R}_{MS}, \quad (51)$$

and

$$\triangle\tilde{R}\Big|_{\max} = \max \left\{ \tilde{R}_{MSF} - \tilde{R}_{MS} \right\}, \quad (52)$$

where $\tilde{R}_{MSF}$ and $\tilde{R}_{MS}$ denote the total number of bits carried by the N_{sc} subcarriers using MSF-STSK and OFDM-MS-STSK, respectively, using both AC indexing and FI indexing without taking the STSK codeword into consideration, while $\triangle\tilde{R}$ is the difference between both numbers. The values of $\tilde{R}_{MSF}$ and $\tilde{R}_{MS}$ can be expressed as

$$\tilde{R}_{MSF} = \frac{N_{sc}}{N_B} \left\{ (N_B - 1)\log_2(N_{AC}) + \log_2(N_B N_{FI}) \right\}, \quad (53)$$

and

$$\tilde{R}_{MS} = \left(\frac{N_{sc}}{N_B} \right) N_B \log_2(N_{AC}). \quad (54)$$

Hence, we have

$$\triangle\tilde{R} = \left(\frac{N_{sc}}{N_B} \right) \log_2 \left(\frac{N_{FI}}{N_{AC}} N_B \right). \quad (55)$$

In general, the numbers of ACs, N_{AC} and N_{FI}, dedicated for MS and FI encoding is limited by the number of TAAs and the size of the STSK codeword M, which means that their values are constant for a specific transmitter configuration. Therefore, we can modify the size of the block to satisfy (52) by determining the maximum value of $\triangle\tilde{R}$ in terms of N_B as

$$\frac{\partial \triangle\tilde{R}}{\partial N_B} = 0, \quad (56)$$

where

$$\frac{\partial \triangle\tilde{R}}{\partial N_B} = \frac{N_{sc}}{N_B^2} \log_2 \left(\frac{N_{AC}}{N_{FI}} N_B \right) + \frac{N_{sc}}{N_B^2 \log_e(2)}. \quad (57)$$

Now, by combining (56) and (57) we get

$$\log_2 \left(N_B \frac{N_{FI}}{N_{AC}} \right) + \frac{1}{\log_e(2)} = 0, \quad (58)$$

$$\log_2(N_B) = \frac{1}{\log_e(2)} + \log_2 \left(\frac{N_{AC}}{N_{FI}} \right), \quad (59)$$

and finally

$$N_B \to \left(\frac{N_{AC}}{N_{FI}} \right) 2^{\frac{1}{\log_e(2)}}. \quad (60)$$

The best block size N_B of MSF-STSK for different values of N_{AC}/N_{FI} is shown in Figure 16. Given that (60) results in a decimal number, the number of subcarriers per block scales down or up to the nearest integer power of two.

For example, consider an MSF-STSK system associated with $N^t_{RF} = 4$ TAAs, $M = 2$, $N_{sc} = 8192$ subcarriers. The total number of ACs is 6, where the first four ACs

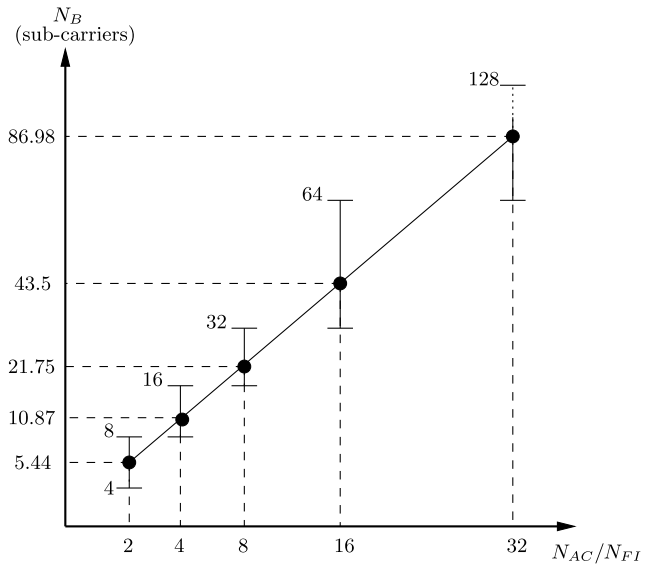

FIGURE 16. Optimal values of N_B versus the N_{AC}/N_{FI} ratio.

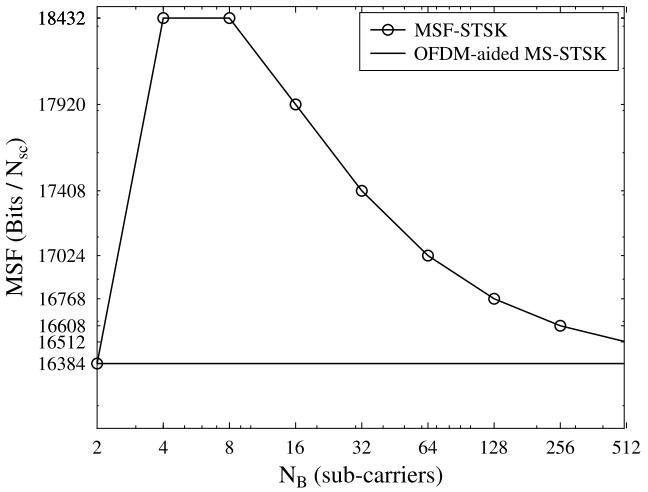

FIGURE 17. Number of bits conveyed by ACs and FI indices per OFDM symbol over N_{sc} subcarriers versus N_B.

are dedicated to the MS-STSK component associated with $N_{AC} = 4$ and the remaining two ACs are used for FI encoding. The number of bits conveyed by ACs and FI indices per OFDM symbol over N_{sc} subcarriers versus N_B is shown in Figure 17. The optimal block size is either $N_B = 4$ or 8, where an extra 2048 bits per STSK-OFDM symbol may be carried via the FI blocks. However, the optimal size of the block here is $N_B = 4$, since it will be shown in the following section that it has a lower complexity order at the same throughput.

D. MSF-STSK COMPLEXITY

The complexity order of the OFDM-MS-STSK detector for each codeword detected at each subcarrier is $\bar{\mathcal{O}}_{MS-STSK}(M_Q M_c N_{AC})$ [18], which can be reduced to $\mathcal{O}_{MS-STSK}(M_Q N_{AC})$ when employing the HL-ML detector shown in (28). However, in conjunction with MSF-STSK, the complexity order is increased as a result of increasing the throughput with the aid of an extra search space, which is the FI.

Given that the MSF-STSK detector applies full search over a block of N_B subcarriers in two consecutive stages for the sake of detecting the transmitted MSF-STSK symbols, the complexity order per block of an ML optimal detector is defined as

$$\bar{\mathcal{O}}_{MSF}^{N_B} = N_B N_{FI} M_Q M_c \tag{61}$$

$$+ (N_B - 1) M_Q M_c N_{AC}, \tag{62}$$

$$= M_Q M_c \{N_B N_{FI} + N_B N_{AC} - N_{AC}\}, \tag{63}$$

which can be scaled down in the context of single codeword per subcarrier detection to

$$\bar{\mathcal{O}}_{MSF} = M_Q M_c \left\{ N_{FI} + N_{AC}(1 - \frac{1}{N_B}) \right\}. \tag{64}$$

Furthermore, by employing the HL-ML detector of (44) and (46) for both stages, the complexity order per block is reduced to

$$\mathcal{O}_{MSF}^{N_B} = M_Q \{N_B N_{FI} + N_B N_{AC} - N_{AC}\}, \tag{65}$$

while the complexity order per codeword/subcarrier to

$$\mathcal{O}_{MSF} = M_Q \left\{ N_{FI} + N_{AC}(1 - \frac{1}{N_B}) \right\}. \tag{66}$$

For a given number of subcarriers N_{sc}, employing the MSF-STSK scheme would enhance the throughput of the OFDM-MS-STSK scheme at the cost of an increased complexity order. Using the same example as in Section III-C, choosing $N_B = 4$ or $N_B = 8$ would achieve the same throughput. However, the complexity order of $\bar{\mathcal{O}}_{MSF}^{N_B=8}$ is higher than $\bar{\mathcal{O}}_{MSF}^{N_B=4}$. Hence, based on the configurations specified in this example, the block size of $N_B = 4$ is preferable.

E. PERFORMANCE RESULTS

The simulation parameters used in this section are the same as those used for the OFDM-MS-STSK system summarized in Table 5. Figure 18 shows the performance of the MSF-STSK system for different configurations for transmission over the mmWave wideband channel. Given that all systems have $N_{AC} = 4$ ACs for the MS-STSK component of MSF-STSK, the block size of each of the MSF-STSK systems considered was chosen based on Sections III-C and III-D, where MSF-STSK associated with $N_{RF}^t = 8$ should have a block size of $N_B = 16$ when using only $N_{FI} = 2$ ACs for frequency indexing, the MSF-STSK arrangement associated with $N_{RF}^t = 6$ should have a block size of $N_B = 4$, when $N_{FI} = 4$ ACs are employed for frequency indexing. By contrast, the MSF-STSK associated with $N_{RF}^t = 4$ should have a block size of $N_B = 4$ when using only $N_{FI} = 2$ ACs for frequency indexing. At a given number of ACs for MS and FI, these configurations were selected for achieving detection at the lowest possible complexity order.

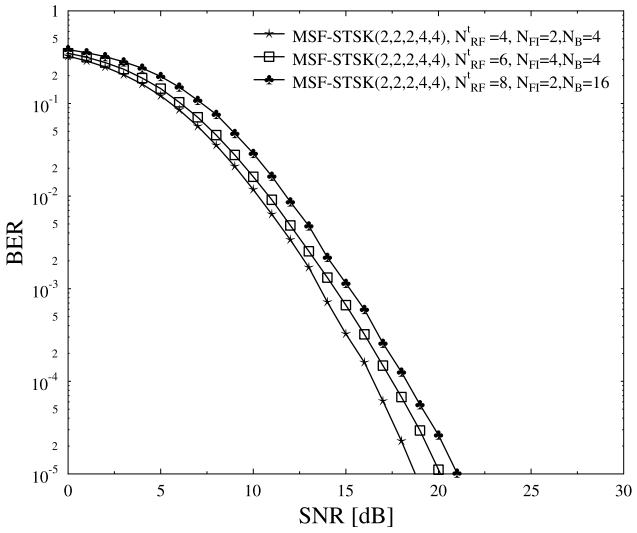

FIGURE 18. BER performance of the MSF-STSK system with different transmitter configuration and HL-ML detection employed at the receiver.

The number of bits transmitted over the MS-STSK component of the system is equal to 32,768 spread over 8,192 subcarriers, which are divided into 2 bits, 2 bits and 2 bits conveyed by the dispersion matrix, the modulated symbol and the AC over each subcarrier, respectively. However, the three systems of Figure 18 have a total of $N_{RF}^t = 4$, $N_{RF}^t = 6$ and $N_{RF}^t = 8$ transmit antennas in conjunction with $N_{FI} = 2$, $N_{FI} = 4$ and $N_{FI} = 2$ ACs employed for frequency indexing, each with $N_B = 4$, $N_B = 4$ and $N_B = 16$ subcarriers per block. Hence, they can convey 6, 144, 8, 192 and 2, 560 extra bits over the 8, 192 subcarriers using frequency indexing, respectively. Furthermore, the BER performance can be enhanced by applying ABF with the aid of adding multiple AEs at each of the TAAs and the RAAs at the transmitter and receiver. Note that the MSF-STSK systems considered in this section were not compared to their equivalent-throughput OFDM-MS-STSK counterparts, since for the considered configurations no equivalent-throughput OFDM-MS-STSK systems can be employed.

IV. CONCLUSIONS

In this paper we proposed a novel OFDM-MS-STSK system for communications over mmWaves, which strikes a flexible trade-off between the attainable throughput and the achievable diversity gain. This system sub-divides the overall bandwidth into a high number of subcarriers, where a single STSK codeword is transmitted over each subcarrier by implicitly carrying the activated AC index. Furthermore, for the sake of mitigating the effect of the high path loss, ABF is employed in conjunction with a pair of phase-shifters and power amplifiers connected to each antenna element, where each antenna array contains multiple antenna elements at both the transmitter and receiver. Furthermore, the OFDM-MS-STSK system was extended to invoke the frequency domain for further enhancing the transmission rate with the aid of frequency indexing in the MSF-STSK system. Due to the large bandwidths available at mmWaves, a high number of subcarriers can be used for OFDM systems, which can be subdivided into blocks in order to spread the transmit information both over space-time-and frequency. The MSF-STSK system is capable of further enhancing the multiplexing gain of the system at the cost of an increased complexity. However, for the sake of reducing the overall detection complexity order, HL-ML was employed for both the OFDM-MS-STSK and MSF-STSK schemes.

REFERENCES

[1] T. S. Rappaport *et al.*, "Millimeter wave mobile communications for 5G cellular: It will work!" *IEEE Access*, vol. 1, pp. 335–349, May 2013.
[2] Z. Pi and F. Khan, "An introduction to millimeter-wave mobile broadband systems," *IEEE Commun. Mag.*, vol. 49, no. 6, pp. 101–107, Jun. 2011.
[3] S. Hur *et al.*, "Proposal on millimeter-wave channel modeling for 5G cellular system," *IEEE J. Sel. Topics Signal Process.*, vol. 10, no. 3, pp. 454–469, Apr. 2016.
[4] G. R. Maccartney, T. S. Rappaport, M. K. Samimi, and S. Sun, "Millimeter-wave omnidirectional path loss data for small cell 5G channel modeling," *IEEE Access*, vol. 3, pp. 1573–1580, Sep. 2015.
[5] S. Hur, T. Kim, D. J. Love, J. V. Krogmeier, T. A. Thomas, and A. Ghosh, "Millimeter wave beamforming for wireless backhaul and access in small cell networks," *IEEE Trans. Commun.*, vol. 61, no. 10, pp. 4391–4403, Oct. 2013.
[6] L. Hanzo, M. El-Hajjar, and O. Alamri, "Near-capacity wireless transceivers and cooperative communications in the MIMO era: Evolution of standards, waveform design, and future perspectives," *Proc. IEEE*, vol. 99, no. 8, pp. 1343–1385, Aug. 2011.
[7] P. W. Wolniansky, G. J. Foschini, G. D. Golden, and R. A. Valenzuela, "V-BLAST: An architecture for realizing very high data rates over the rich-scattering wireless channel," in *Proc. URSI Int. Symp. Signals, Syst., Electron.*, Oct. 1998, pp. 295–300.
[8] S. Alamouti, "A simple transmit diversity technique for wireless communications," *IEEE J. Sel. Areas Commun.*, vol. 16, no. 8, pp. 1451–1458, Oct. 1998.
[9] V. Tarokh, H. Jafarkhani, and A. R. Calderbank, "Space-time block codes from orthogonal designs," *IEEE Trans. Inf. Theory*, vol. 45, no. 5, pp. 1456–1467, Jul. 1999.
[10] L. Hanzo, T. Liew, B. Yeap, R. Tee, and S. Ng, *Turbo Coding, Turbo Equalisation Space-Time Coding: EXIT-Chart-Aided Near-Capacity Designs for Wireless Channels*. Hoboken, NJ, USA: Wiley, 2011. [Online]. Available: https://books.google.co.uk/books?id=i0gRC0wGVFgC
[11] R. Y. Mesleh, H. Haas, S. Sinanovic, C. W. Ahn, and S. Yun, "Spatial modulation," *IEEE Trans. Veh. Technol.*, vol. 57, no. 4, pp. 2228–2241, Jul. 2008.
[12] P. Yang, M. D. Renzo, Y. Xiao, S. Li, and L. Hanzo, "Design guidelines for spatial modulation," *IEEE Commun. Surveys Tut.*, vol. 17, no. 1, pp. 6–26, 1st Quart., 2015.
[13] P. Yang *et al.*, "Single-carrier SM-MIMO: A promising design for broadband large-scale antenna systems," *IEEE Commun. Surveys Tut.*, vol. 18, no. 3, pp. 1687–1716, 3rd Quart., 2016.
[14] P. Liu and A. Springer, "Space shift keying for los communication at mmWave frequencies," *IEEE Wireless Commun. Lett.*, vol. 4, no. 2, pp. 121–124, Apr. 2015.
[15] L. L. Hanzo, O. Alamri, M. El-Hajjar, and N. Wu, *Near-Capacity Multi-Functional MIMO Systems: Sphere-Packing, Iterative Detection Cooperation*. Hoboken, NJ, USA: Wiley, 2009. [Online]. Available: http://books.google.co.uk/books?id=590-JItOJREC
[16] M. El-Hajjar, O. Alamri, J. Wang, S. Zummo, and L. Hanzo, "Layered steered space-time codes using multi-dimensional sphere packing modulation," *IEEE Trans. Wireless Commun.*, vol. 8, no. 7, pp. 3335–3340, Jul. 2009.
[17] S. Sugiura, S. Chen, and L. Hanzo, "Space-time shift keying: A unified MIMO architecture," in *Proc. IEEE Global Telecommun. Conf.*, Dec. 2010, pp. 1–5.

[18] I. A. Hemadeh, M. El-Hajjar, S. Won, and L. Hanzo, "Multi-set space-time shift-keying with reduced detection complexity," *IEEE Access*, vol. 4, pp. 4234–4246, 2016.

[19] I. A. Hemadeh, M. El-Hajjar, S. Won, and L. Hanzo, "Layered multi-group steered space-time shift-keying for millimeter-wave communications," *IEEE Access*, vol. 4, pp. 3708–3718, 2016.

[20] S. Sun, T. S. Rappaport, R. W. Heath, Jr., A. Nix, and S. Rangan, "MIMO for millimeter-wave wireless communications: Beamforming, spatial multiplexing, or both?" *IEEE Commun. Mag.*, vol. 52, no. 12, pp. 110–121, Dec. 2014.

[21] O. El Ayach, S. Rajagopal, S. Abu-Surra, Z. Pi, and R. W. Heath, Jr., "Spatially sparse precoding in millimeter wave MIMO systems," *IEEE Trans. Wireless Commun.*, vol. 13, no. 3, pp. 1499–1513, Mar. 2014.

[22] S. Kutty and D. Sen, "Beamforming for millimeter wave communications: An inclusive survey," *IEEE Commun. Surveys Tut.*, vol. 18, no. 2, pp. 949–973, 2nd Quart., 2016.

[23] T. S. Rappaport, J. N. Murdock, and F. Gutierrez, Jr., "State of the art in 60-GHz integrated circuits and systems for wireless communications," *Proc. IEEE*, vol. 99, no. 8, pp. 1390–1436, Aug. 2011.

[24] S. Sugiura and L. Hanzo, "Single-RF spatial modulation requires single-carrier transmission: Frequency-domain turbo equalization for dispersive channels," *IEEE Trans. Veh. Technol.*, vol. 64, no. 10, pp. 4870–4875, Oct. 2015.

[25] E. Başar, U. Aygölü, E. Panayırcı, and H. V. Poor, "Orthogonal frequency division multiplexing with index modulation," *IEEE Trans. Signal Process.*, vol. 61, no. 22, pp. 5536–5549, Nov. 2013.

[26] M. Wen, X. Cheng, M. Ma, B. Jiao, and H. V. Poor, "On the achievable rate of OFDM with index modulation," *IEEE Trans. Signal Process.*, vol. 64, no. 8, pp. 1919–1932, Apr. 2016.

[27] B. Zheng, F. Chen, M. Wen, F. Ji, H. Yu, and Y. Liu, "Low-complexity ML detector and performance analysis for OFDM with in-phase/quadrature index modulation," *IEEE Commun. Lett.*, vol. 19, no. 11, pp. 1893–1896, Nov. 2015.

[28] N. Ishikawa, S. Sugiura, and L. Hanzo, "Subcarrier-index modulation aided OFDM—Will it work?" *IEEE Access*, vol. 4, pp. 2580–2593, 2016.

[29] H. Zhang, L.-L. Yang, and L. Hanzo, "Compressed sensing improves the performance of subcarrier index-modulation-assisted OFDM," *IEEE Access*, vol. 4, pp. 7859–7873, 2016.

[30] T. Datta, H. S. Eshwaraiah, and A. Chockalingam, "Generalized space-and-frequency index modulation," *IEEE Trans. Veh. Technol.*, vol. 65, no. 7, pp. 4911–4924, Jul. 2016.

[31] H. A. Ngo, C. Xu, S. Sugiura, and L. Hanzo, "Space-time-frequency shift keying for dispersive channels," *IEEE Signal Process. Lett.*, vol. 18, no. 3, pp. 177–180, Mar. 2011.

[32] M. I. Kadir, S. Sugiura, S. Chen, and L. Hanzo, "Unified MIMO-multicarrier designs: A space–time shift keying approach," *IEEE Commun. Surveys Tut.*, vol. 17, no. 2, pp. 550–579, 2nd Quart., 2015.

[33] S. Sugiura, S. Chen, and L. Hanzo, "Coherent and differential space-time shift keying: A dispersion matrix approach," *IEEE Trans. Commun.*, vol. 58, no. 11, pp. 3219–3230, Nov. 2010.

[34] M. K. Samimi and T. S. Rappaport, "Ultra-wideband statistical channel model for non line of sight millimeter-wave urban channels," in *Proc. IEEE Global Commun. Conf. (GLOBECOM)*, Dec. 2014, pp. 3483–3489.

[35] T. S. Rappaport, G. R. Maccartney, M. K. Samimi, and S. Sun, "Wideband millimeter-wave propagation measurements and channel models for future wireless communication system design," *IEEE Trans. Commun.*, vol. 63, no. 9, pp. 3029–3056, Sep. 2015.

[36] H. Xu, T. S. Rappaport, R. J. Boyle, and J. H. Schaffner, "Measurements and models for 38-GHz point-to-multipoint radiowave propagation," *IEEE J. Sel. Areas Commun.*, vol. 18, no. 3, pp. 310–321, Mar. 2000.

[37] B. Razavi, "A 60-GHz CMOS receiver front-end," *IEEE J. Solid-State Circuits*, vol. 41, no. 1, pp. 17–22, Jan. 2006.

[38] M. C. Lee, W. H. Chung, and T. S. Lee, "Generalized precoder design formulation and iterative algorithm for spatial modulation in MIMO systems with CSIT," *IEEE Trans. Commun.*, vol. 63, no. 4, pp. 1230–1244, Apr. 2015.

[39] M. K. Samimi and T. S. Rappaport, "3-D statistical channel model for millimeter-wave outdoor mobile broadband communications," in *Proc. IEEE Int. Conf. Commun. (ICC)*, Jun. 2015, pp. 2430–2436.

[40] M. K. Samimi and T. S. Rappaport, "Local multipath model parameters for generating 5G millimeter-wave 3GPP-like channel impulse response," in *Proc. 10th Eur. Conf. Antennas Propag. (EuCAP)*, Apr. 2016, pp. 1–5.

[41] A. Maltsev *et al.* (May 2010). *Channel Models for 60 GHz WLAN Systems*. [Online]. Available: http://www.ieee802.org/11/Reports/tgad_update.htm

[42] IEEE. (Oct. 2009). *IEEE WPAN 802.15.3c Millimeter-Wave Based Alternative Physical Layer Extension*. [Online]. Available: http://www.ieee802.org/15/pub/TG3c.html

[43] G. R. Maccartney, T. S. Rappaport, S. Sun, and S. Deng, "Indoor office wideband millimeter-wave propagation measurements and channel models at 28 and 73 GHz for ultra-dense 5G wireless networks," *IEEE Access*, vol. 3, pp. 2388–2424, 2015.

[44] M. Driusso, F. Babich, M. I. Kadir, and L. Hanzo, "OFDM aided space-time shift keying for dispersive downlink channels," in *Proc. IEEE Veh. Technol. Conf. (VTC)*, Sep. 2012, pp. 1–5.

[45] M. Kadir, S. Sugiura, J. Zhang, S. Chen, and L. Hanzo, "OFDMA/SC-FDMA aided space–time shift keying for dispersive multiuser scenarios," *IEEE Trans. Veh. Technol.*, vol. 62, no. 1, pp. 408–414, Jan. 2013.

[46] M. Kadir, S. Chen, and L. Hanzo, "A reduced-complexity detector for OFDMA/SC-FDMA-aided space-time shift keying," in *Proc. IEEE 78th Veh. Technol. Conf. (VTC)*, Sep. 2013, pp. 1–5.

IBRAHIM A. HEMADEH (S'15) received the B.Eng. degree (Hons.) in computer and communications engineering from Islamic University of Lebanon in 2010, the M.Sc. degree (Hons.) in wireless communications from the University of Southampton, U.K., in 2012, where he is currently pursuing the Ph.D. degree in wireless communications under the supervision of Prof. L. Hanzo and Dr. M. El-Hajjar. His research interests mainly include mmWave communications, multifunctional MIMO, and multiuser MIMO.

MOHAMMED EL-HAJJAR received the B.Eng. degree in electrical engineering from the American University of Beirut, Lebanon, in 2004, and the M.Sc. degree in radio frequency communication systems and the Ph.D. degree in wireless communications from the University of Southampton, U.K., in 2005 and 2008, respectively.

He was with Imagination Technologies as a Design Engineer, where he was involved in designing and developing Imagination's multi-standard communications platform, which resulted in three patents. In 2012, he was a Lecturer of Electronics and Computer Science with the Southampton Wireless Research Group, University of Southampton, where he is currently a Lecturer. He has published a Wiley-IEEE book and in excess of 60 journal and international conference papers. His research interests are mainly in the development of intelligent communications systems, including energy-efficient transceiver design, MIMO, mmWave communications, and radio-over-fiber systems.

Dr. Hajja received several academic awards, including the Dean's Award for creative achievement, the Dorothy Hodgkin Postgraduate Award, and the IEEE ICC 2010 Best Paper Award.

SEUNGHWAN WON (M'04–SM'10) received the B.S. and M.S. degrees in radio science and engineering from Korea University, Seoul, South Korea, in 1999 and 2001, respectively. He is currently pursuing the Ph.D. degree with the Communications Research Group, School of Electronics and Computer Science, University of Southampton, U.K.

He was a Research Engineer with the Mobile Communication Technology Research Laboratory, LG Electronics R&D, from 2001 to 2004. He was with Samsung between 2008 and 2013. In 2013, he was an Associate Professor with the University of Southampton, where he is currently a Teacher and Researcher with the University of Southampton in Johor, Malaysia. He published a host of papers in his research fields. His major research interests include initial synchronization in noncoherent MIMO aided single- and multi-carrier CDMA, IDMA, and OFDMA, and in iterative synchronization schemes designed for MIMO aided single- and multi-carrier transmission systems.

Dr. Won received the 2004 State Scholarship of the Information and Telecommunication National Scholarship Program, the Ministry of Information and Communication, South Korea.

LAJOS HANZO (M'90–SM'91–F'04) received the master's degree in electronics, the Ph.D. and Doctor Honoris Causa degrees from Budapest University of Technology and Economics, in 1976, 1983, and 2009, respectively, and the Doctor Honoris Causa degree from the University of Edinburgh, in 2015.

During his 40-year career in telecommunications, he has held various research and academic positions in Hungary, Germany, and the U.K. Since 1986, he has been with the School of Electronics and Computer Science, University of Southampton, U.K., as the Chair of Telecommunications. He has successfully supervised 110 Ph.D. students, co-authored 20 John Wiley/IEEE Press books in mobile radio communications, totaling in excess of 10,000 pages, co-authored over 1,600 research contributions found at the IEEE Xplore, acted as the TPC Chair and General Chair of the IEEE conferences, presented keynote lectures, and received a number of distinctions. He is directing a 60-strong academic research team, involved in a range of research projects in the field of wireless multimedia communications sponsored by the industry, the Engineering and Physical Sciences Research Council, U.K., the European Research Councils Advanced Fellow Grant, and the Royal Societies Wolfson Research Merit Award. He is an Enthusiastic Supporter of Industrial and Academic Liaison and offers a range of industrial courses.

Dr. Hanzo is a fellow of the Royal Academy of Engineering, the Institution of Engineering and Technology, and the European Association for Signal Processing. He is also a Governor of the IEEE ComSoc and of VTS. From 2008 to 2012, he was an Editor-in-Chief of the IEEE Press and a Chaired Professor with Tsinghua University, Beijing. He has more than 25,000 citations.